

# Sensitivity analysis of the potential impact of discrepancies in stratosphere-troposphere exchange on inferred sources and sinks of CO<sub>2</sub>

F. Deng<sup>1</sup>, D. B. A. Jones<sup>1,2</sup>, T. W. Walker<sup>1</sup>, M. Keller<sup>1</sup>, K. W. Bowman<sup>3,2</sup>, D. K. Henze<sup>4</sup>, R. Nassar<sup>5</sup>, E. A. Kort<sup>6</sup>, S. C. Wofsy<sup>7</sup>, K. A. Walker<sup>1</sup>, A. E. Bourassa<sup>8</sup>, D. A. Degenstein<sup>8</sup>

[1]{Department of Physics, University of Toronto, Toronto, ON, Canada}

[2]{Joint Institute for Regional Earth System Science and Engineering, University of California, Los Angeles, CA, USA}

[3]{Jet Propulsion Laboratory, California Institute of Technology, Pasadena, CA, USA}

[4]{Department of Mechanical Engineering, University of Colorado, Boulder, CO, USA}

[5]{Climate Research Division, Environment Canada, Toronto, ON, Canada}

[6]{Department of Atmospheric, Oceanic and Space Sciences, University of Michigan, Ann Arbor, MI, USA}

[7]{Harvard University, Cambridge, MA, USA}

[8]{Institute of Space and Atmospheric Studies, University of Saskatchewan, Saskatoon, Canada}

## Abstract

The upper troposphere and lower stratosphere (UTLS) represents a transition region between the more dynamically active troposphere and more stably stratified stratosphere. The region is characterized by strong gradients in the distribution of long-lived tracers, whose representation in models is sensitive to discrepancies in transport. We evaluate the GEOS-Chem model in the UTLS using carbon dioxide (CO<sub>2</sub>) and ozone (O<sub>3</sub>) observations from the HIAPER (The High-Performance Instrumented Airborne Platform for Environmental Research) Pole-to-Pole Observations (HIPPO) campaign in March 2010. GEOS-Chem CO<sub>2</sub>/O<sub>3</sub> correlation suggests that

1 there is a discrepancy in mixing across the tropopause in the model, which results in an  
2 overestimate of CO<sub>2</sub> and an underestimate of O<sub>3</sub> in the Arctic lower stratosphere. We assimilate  
3 stratospheric O<sub>3</sub> data from the Optical Spectrograph and InfraRed Imager System (OSIRIS) and  
4 use the assimilated O<sub>3</sub> fields together with the HIPPO CO<sub>2</sub>/O<sub>3</sub> correlations to obtain an  
5 adjustment to the modeled CO<sub>2</sub> profile in the Arctic UTLS (primarily between the 320 K and 360  
6 K isentropic surfaces). The HIPPO-derived adjustment corresponds to a sink of 0.60 Pg C for  
7 March – August 2010 in the Arctic. Imposing this adjustment results in a reduction in the CO<sub>2</sub>  
8 sinks inferred from GOSAT observations for temperate North America, Europe, and tropical  
9 Asia of 19%, 13%, and 49%, respectively. Conversely, the inversion increased the source of CO<sub>2</sub>  
10 from tropical South America by 23%. We find that the model also underestimates CO<sub>2</sub> in the  
11 upper tropical and subtropical troposphere. Correcting for the underestimate in the model relative  
12 to HIPPO in the tropical upper troposphere leads to a reduction in the source from tropical South  
13 America by 77%, and produces an estimated sink for tropical Asia that is only 19% larger than  
14 the standard inversion (without the imposed source and sink). Globally, the inversion with the  
15 Arctic and tropical adjustment produces a sink of -6.64 Pg C, which is consistent with the  
16 estimate of -6.65 Pg C in the standard inversion. However, the standard inversion produces a  
17 stronger northern land sink by 0.98 Pg C to account for the CO<sub>2</sub> overestimate in the high-latitude  
18 UTLS, suggesting that this UTLS discrepancy can impact the latitudinal distribution of the  
19 inferred sources and sinks. We find that doubling the model resolution from 4° x 5° to 2° x 2.5°  
20 enhances the CO<sub>2</sub> vertical gradient in the high-latitude UTLS, and reduces the overestimate in  
21 CO<sub>2</sub> in the extratropical lower stratosphere. Our results illustrate that discrepancies in the CO<sub>2</sub>  
22 distribution in the UTLS can affect CO<sub>2</sub> flux inversions and suggest the need for more careful  
23 evaluation of model errors in the UTLS.

24

25

## 26 **1 Introduction**

27 The Greenhouse Gases Observing Satellite (GOSAT), the first satellite launched specifically to  
28 monitor atmospheric carbon dioxide (CO<sub>2</sub>) from space, has been providing greater observational  
29 coverage of atmospheric CO<sub>2</sub> than is possible from existing surface observation networks. The  
30 expectation has been that these data would offer greater constraints on atmospheric CO<sub>2</sub>, and  
31 hence improve estimates of regional sources and sinks of CO<sub>2</sub>. However, although global flux

1 estimates from various inversion analyses constrained by GOSAT data have been found to be  
2 consistent across the different inversion analyses, and in good agreement with optimized fluxes  
3 based on flask CO<sub>2</sub> measurements, regional flux estimates have not been robust (e.g. Maksyutov  
4 et al., 2013; Basu et al., 2013; Chevallier et al., 2014; Deng et al., 2014). Deng et al. (2014), for  
5 example, found that flux estimates for temperate North America and tropical South America  
6 were particularly sensitive to the treatment of the regional bias in the GOSAT data. Chevallier et  
7 al. (2014) showed that model errors are another source of discrepancy in the regional fluxes  
8 inferred from GOSAT CO<sub>2</sub> data.

9 Inversion analyses using satellite observations have also produced large differences in the flux  
10 estimates from some regions, such as Europe and Northern Africa, relative to those inferred from  
11 the surface-observing network. Reuter et al. (2014) noted that the satellite-derived flux estimates  
12 for Europe are more than a factor of two larger than those obtained from in situ surface data. It is  
13 difficult to determine whether the differences between the fluxes inferred from the satellite data  
14 and those based on the surface data reflect actual additional information provided by the satellite  
15 data or discrepancies in the free troposphere in the models, to which the surface data would be  
16 much less sensitive.

17 Observations from instruments such as GOSAT and the Orbiting Carbon Observatory 2 (OCO-2)  
18 are vertically integrated column abundances of CO<sub>2</sub> (referred to as XCO<sub>2</sub>), and it is expected that  
19 inversion analyses using these data will be less sensitive to vertical transport errors, such as  
20 mixing in the planetary boundary layer (PBL), than those using in situ surface data. However,  
21 Lauvaux and Davis (2014) found that vertical transport errors are still an issue for inversion  
22 analyses using column data. Stephens et al. (2007) showed that models that do not correctly  
23 capture the vertical transport of CO<sub>2</sub> between the PBL and the free troposphere, and,  
24 consequently, overestimate the vertical gradient in CO<sub>2</sub>, and tend to suggest a stronger extra-  
25 tropical land sink of CO<sub>2</sub>. It is unclear how sensitive the XCO<sub>2</sub>-based inversions are to model  
26 errors in transport in the free troposphere. We examine here the potential impact of discrepancies  
27 in CO<sub>2</sub> in the upper troposphere and lower stratosphere (UTLS) on the regional flux estimates  
28 inferred from GOSAT XCO<sub>2</sub> data. We focus on the UTLS because this is a region that has been  
29 neglected as an important source of error in CO<sub>2</sub> flux inversions, even though it is characterized  
30 by strong vertical gradients in the distribution of long-lived tracers and by complex transport

1 processes that occur on a range of spatial and temporal scales that can be challenging for models  
2 to reliably capture.

3 In the extratropics, the latitudinal distribution of CO<sub>2</sub> is strongly influenced by quasi-adiabatic  
4 transport that tends to align the CO<sub>2</sub> distribution along the isentropes (although diabatic effects  
5 result in cross-isentropic transport) (Miyazaki et al., 2008). This can be seen in Fig. 1, which  
6 shows the zonal mean CO<sub>2</sub> distribution on April 1, 2010 estimated using the GEOS-Chem  
7 model. Also shown are the isentropic surfaces in the model. In the tropics, convective transport  
8 provides a means for fast transport of CO<sub>2</sub> from the lower to the upper troposphere. In the  
9 extratropics, isentropic transport plays an important role in the export of air from the PBL to the  
10 free troposphere. Parazoo et al. (2012) showed that not properly capturing this isentropic  
11 transport of CO<sub>2</sub> could impact CO<sub>2</sub> flux inversions. They conducted an observing system  
12 simulation experiment (OSSE) and found that data gaps in satellite measurements due to cloud  
13 cover, which is associated with poleward moist transport at mid-latitudes, could produce large  
14 biases in regional flux estimates. For example, in their perfect model OSSE, the sampling bias  
15 due to the data gaps resulted in a bias of 0.43 Pg C yr<sup>-1</sup> for the European flux estimates. Here we  
16 focus mainly on transport in the extratropical UTLS, where mixing along isentropic surfaces,  
17 such as the 320 K and the 340 K surfaces, enables rapid exchange of CO<sub>2</sub> between the high  
18 latitude UTLS and the subtropical and mid-latitude middle and upper troposphere. Miyazaki et  
19 al. (2008) showed that in winter and spring, transport by large-scale eddies has a positive  
20 tendency on CO<sub>2</sub> in the high-latitude UTLS, transporting air with high CO<sub>2</sub> from the lower  
21 troposphere at lower latitudes. In contrast, transport by the mean meridional circulation has a  
22 negative tendency on CO<sub>2</sub> in the high-latitude UTLS, due to the transport of low CO<sub>2</sub> air from  
23 the tropical upper troposphere and down from the high-latitude stratosphere. Accurately  
24 reproducing the observed CO<sub>2</sub> distribution in the UTLS requires models to reliably capture the  
25 compensating effects of these transport processes. The CO<sub>2</sub> distribution will also be influenced  
26 by discrepancies in the numerical schemes and in the parameterizations of subgrid-scale  
27 processes not explicitly represented in the models.

28 We use observations of CO<sub>2</sub> and ozone (O<sub>3</sub>) from the HIAPER Pole-to-Pole Observations  
29 (HIPPO) campaign to evaluate the GEOS-Chem CO<sub>2</sub> simulation in the high-latitude UTLS. The  
30 GEOS-Chem model has been widely used as a tropospheric chemistry transport model (CTM),  
31 but it is driven by assimilated meteorological fields from the Global Modeling and Assimilation

1 Office (GMAO) that extend from the surface to 0.01 hPa, providing a full description of the  
2 circulation in the stratosphere. The model simulates a source of ozone from the stratosphere to  
3 the troposphere of about 500 Tg O<sub>3</sub>/yr, which is consistent with the multi-model mean of 550 Tg  
4 O<sub>3</sub>/yr from Stevenson et al. (2006). However, although the model has been successfully used for  
5 studies of tropospheric chemistry and transport, we note the CO<sub>2</sub> flux inversions are particularly  
6 sensitive to model errors. As discussed below, we find that the model overestimates CO<sub>2</sub> relative  
7 to the HIPPO data in the high-latitude UTLS. We then use the HIPPO CO<sub>2</sub>/O<sub>3</sub> correlations to  
8 impose an adjustment to the modeled CO<sub>2</sub> in the high-latitude UTLS and conduct a series of  
9 inversion analyses of the GOSAT data, using the GEOS-Chem 4-dimensional variational (4D-  
10 var) data assimilation system, to quantify the potential impact of the UTLS adjustment in CO<sub>2</sub> on  
11 regional flux estimates of CO<sub>2</sub>.

12 We begin in Section 2 with a brief discussion of the data and the methods. We use the same  
13 GOSAT data and 4D-var inversion approach as in Deng et al. (2014). In Section 3, we present  
14 our results, starting with a discussion of the use of the HIPPO CO<sub>2</sub>/O<sub>3</sub> correlations to evaluate  
15 the model in the UTLS, followed by results of the 4D-var inversion analyses. Finally, we  
16 conclude with a discussion of the implications of our results in Section 4.

17

## 18 **2 Data and Methods**

### 19 **2.1 Data Sets**

20 We use here the NASA Atmospheric CO<sub>2</sub> Observations from Space (ACOS) GOSAT CO<sub>2</sub> data  
21 product (version b2.10) (O'Dell et al., 2012), spanning July 2009 to December 2010. The ACOS  
22 retrievals employ an optimal estimation approach to infer profile abundances of CO<sub>2</sub> from the  
23 measurements of reflected short wave infrared (SWIR) solar radiation made by the Thermal and  
24 Near-infrared Sensor for carbon Observation Fourier Transform Spectrometer (TANSO-FTS)  
25 onboard the GOSAT satellite. The retrieved CO<sub>2</sub> is the total column dry-air mole fraction  
26 (XCO<sub>2</sub>); consequently, when the data were assimilated into the model, the modeled fields are  
27 converted to XCO<sub>2</sub> using the reported GOSAT a priori profile, column averaging kernel, and  
28 pressure weighting function. The GOSAT data used here are the same as those labeled  
29 “RUN\_C” in Deng et al. (2014). We use only the “High gain” (H-gain) data, which excludes

1 data over bright surfaces, such as deserts. We also neglect glint observations, which provide  
2 coverage over oceans, since the biases in the glint data are not as well-characterized in version  
3 b2.10 of the ACOS product. For additional details of the dataset we refer the reader to Deng et  
4 al. (2014).

5 To evaluate the model simulation, we use data from the HIPPO aircraft campaign from March –  
6 April 2010 (campaign 3). HIPPO-3 sampled the atmosphere across the Pacific Ocean, from near  
7 the North Pole to the coastal region of Antarctica, and from the surface to 14 km (Wofsy et al.,  
8 2012). The altitudes of the flights were mostly below 9 km, but extended up toward 14 km  
9 typically at least at the beginning and end of every flight. We focus here on data from the polar  
10 flights on March 26-27, 2010, when there were two profiles that extended up to about 14 km in the  
11 Arctic. The data used here are from the 10-second averaged dataset. The CO<sub>2</sub> data are from two  
12 (harmonized) sensors: the CO<sub>2</sub> Quantum Cascade Laser Spectrometer (CO<sub>2</sub>-QCLS) and the CO<sub>2</sub>  
13 Observations of the Middle Stratosphere instrument (CO<sub>2</sub>-OMS). The O<sub>3</sub> measurements were made  
14 by an ultraviolet (UV) ozone photometer (Wofsy et al., 2011).

15 We assimilate O<sub>3</sub> data from the Optical Spectrograph and InfraRed Imager System (OSIRIS),  
16 which is a Canadian instrument on the Odin satellite. It was launched in February 2001 into a  
17 600 km circular, Sun-synchronous, near-terminator orbit with an inclination of 97.8° (Llewellyn  
18 et al., 2004). OSIRIS consists of a limb-viewing ultraviolet (UV)-visible imaging spectrograph  
19 that measures scattered sunlight between 280 - 820 nm, and a 3-channel infrared imager  
20 measuring atmospheric airglow emissions near 1.27 and 1.53 μm. Vertical profiles of O<sub>3</sub> are  
21 retrieved from OSIRIS measurements using a multiplicative algebraic reconstruction technique  
22 (Degenstein et al., 2009), with a vertical resolution of about 2 km from the upper troposphere to  
23 65 km. We use version 5.07 of the O<sub>3</sub> data. As a result of the orbit of the satellite, observational  
24 coverage is limited to the summer hemisphere, with near global coverage during the equinoxes  
25 and year-round coverage in the tropics. The mean relative difference between the retrieved O<sub>3</sub>  
26 profiles and those from the Stratospheric Aerosol and Gas Experiment (SAGE) II is less than 5%  
27 between 13.5 – 54.5 km, and less than 3% between 24.5 – 53.5 km (Adams et al., 2013). The  
28 precision is better than 5% between 25 -50 km, but degrades at lower altitudes, increasing to 5 –  
29 15% between 10 – 20 km in the extratropics (Bourassa et al., 2012).

1 The assimilation of the OSIRIS data is evaluated using observations from the Atmospheric  
 2 Chemistry Experiment Fourier Transform Spectrometer (ACE-FTS), which is a high resolution  
 3 Fourier transform spectrometer (Bernath et al., 2005) on the Atmospheric Chemistry Experiment  
 4 (ACE) satellite (also known as SCISAT). SCISAT was launched in August 2003, into a low  
 5 Earth orbit at an altitude of 650 km with an inclination of 74°. ACE-FTS measures infrared  
 6 radiation between 2.2 – 13.3  $\mu\text{m}$  (750 – 4400  $\text{cm}^{-1}$ ) with a resolution of 0.02  $\text{cm}^{-1}$  by solar  
 7 occultation. The retrieval products (Boone et al., 2005) include vertical profiles of numerous  
 8 trace gases ranging from the mid-troposphere up to 150 km depending on the gas. We use  
 9 version 2.2 of the ACE-FTS ozone data. Hegglin et al. (2008) found that the version 2.2 ACE-  
 10 FTS profiles have an effective vertical resolution of 1 km in the UTLS. Validation of the ACE-  
 11 FTS  $\text{O}_3$  data suggested that the relative mean difference between ACE-FTS  $\text{O}_3$  data and  
 12 independent measurements is less than 8% between 16 – 44 km. Hegglin et al. (2008) evaluated  
 13 the data in the UTLS and reported mean differences relative to aircraft and ozonesonde data of  
 14 about 8% in the lower stratosphere and a high bias of 18% in the upper troposphere. We restrict  
 15 our use of the ACE-FTS data to the lower stratosphere.

## 16 **2.2 The GEOS-Chem Model and Assimilation Approach**

17 We use the GEOS-Chem (<http://geos-chem.org>) 4D-var data assimilation system (Henze et al.,  
 18 2007) to infer regional  $\text{CO}_2$  flux estimates. The model is driven by assimilated meteorology from  
 19 the Goddard Earth Observing System (GEOS-5) of the NASA GMAO. The native horizontal  
 20 resolution is  $0.5^\circ \times 0.67^\circ$  with 72 vertical levels from the surface to 0.01 hPa, but we degrade the  
 21 resolution to  $4^\circ \times 5^\circ$  and 47 vertical layers (with the reduction in vertical resolution in the middle  
 22 and upper stratosphere). The GEOS-Chem  $\text{CO}_2$  simulation is described and evaluated in Nassar  
 23 et al. (2010). Details of the model configuration and setup of the 4D-Var system are described in  
 24 Deng et al. (2014). Here we will provide only a brief description of the modeling setup.

25 In the 4D-Var approach, we iteratively minimize a cost function  $J$  as a function of  $\text{CO}_2$  fluxes  
 26 ( $\mathbf{x}$ ),

$$27 \quad J(\mathbf{x}) = \frac{1}{2}(\mathbf{H}(\mathbf{x}) - \mathbf{y}^o)^T \mathbf{S}_o^{-1}(\mathbf{H}(\mathbf{x}) - \mathbf{y}^o) + \frac{1}{2}(\mathbf{x} - \mathbf{x}_a)^T \mathbf{S}_a^{-1}(\mathbf{x} - \mathbf{x}_a) \quad (1)$$

1 where  $\mathbf{y}^o$  is a vector of GOSAT XCO<sub>2</sub> observations and  $\mathbf{S}_o$  and  $\mathbf{S}_a$  are the observational and a  
2 priori error covariance matrices, respectively.  $H$  is the forward atmospheric model ( $\mathbf{y} = H(\mathbf{x})$ ),  
3 which includes the GEOS-Chem simulation of the CO<sub>2</sub> distribution and the transformation of the  
4 modeled CO<sub>2</sub> profile to XCO<sub>2</sub> using the GOSAT averaging kernels and a priori profiles. We  
5 solve for monthly mean fluxes of CO<sub>2</sub> using GOSAT observations from March – August 2010.  
6 Following Deng et al. (2014), the reported observational XCO<sub>2</sub> uncertainties are uniformly  
7 inflated by a factor of 1.175 when the data are ingested into the GEOS-Chem assimilation  
8 system.

9 As described in Deng et al. (2014), the prior CO<sub>2</sub> fluxes ( $\mathbf{x}_a$ ) imposed in the model are: (i)  
10 monthly national fossil fuel and cement manufacture CO<sub>2</sub> emissions from the Carbon Dioxide  
11 Information Analysis Center (CDIAC) (Andres et al., 2011); (ii) monthly shipping emissions of  
12 CO<sub>2</sub> from the International Comprehensive Ocean–Atmosphere Data Set (ICOADS) (Corbett  
13 and Koehler, 2003; Corbett, 2004; Endresen et al., 2004; Endresen et al., 2007); (iii) 3-D aviation  
14 CO<sub>2</sub> emissions (Kim et al., 2007; Wilkerson et al., 2010; Friedl 1997); (iv) monthly mean  
15 biomass burning CO<sub>2</sub> emissions from the Global Fire Emissions Database version 3 (GFEDv3)  
16 (van der Werf et al., 2010); (v) biofuel (heating/cooking) CO<sub>2</sub> emissions estimated by Yevich  
17 and Logan (2003); (vi) the flux of CO<sub>2</sub> across the air–water interface based on the climatology of  
18 monthly ocean–atmosphere CO<sub>2</sub> flux by Takahashi et al. (2009); and (vii) 3-hourly terrestrial  
19 ecosystem exchange produced by the Boreal Ecosystem Productivity Simulator (BEPS) (Chen et  
20 al., 1999), which was driven by NCEP reanalysis data (Kalnay et al., 1996) and remotely sensed  
21 leaf area index (LAI) (Deng et al., 2006). The annual terrestrial ecosystem exchange imposed in  
22 each grid box is neutral (Deng and Chen, 2011). The assumed prior errors (1- $\sigma$ ), specified for  
23 each grid box and each month, are 16% for the fossil fuel emissions, 38% for the biomass  
24 burning emissions, and 44% for the ocean flux. For gross primary production (GPP) and total  
25 ecosystem respiration (TER), we assumed an uncertainty of 22% in each three-hour time step  
26 and in each model grid box.

27 The assimilation of the OSIRIS O<sub>3</sub> data into GEOS-Chem uses the same 4D-var approach as  
28 described in Eq. (1). However, instead of optimizing a model parameter, such as the surface  
29 fluxes of CO<sub>2</sub>, we optimize the O<sub>3</sub> distribution at the beginning of the assimilation period (the  
30 initial conditions) so that the model better matches the OSIRIS data over the assimilation period.



1 For the results presented here, the assimilation period extended from March 20 to April 2, 2010.  
2 The O<sub>3</sub> distribution in GEOS-Chem is simulated with a detailed description of O<sub>3</sub>-NO<sub>x</sub>-  
3 hydrocarbon chemistry in the troposphere, but the version of the model employed here uses a  
4 linearized version of the chemistry in the stratosphere, based on the Linoz scheme from  
5 McLinden et al. (2000). As mentioned above, with the Linoz scheme, the model simulates a  
6 source of tropospheric ozone of about 500 Tg O<sub>3</sub>/yr, which is close to the multi-model mean of  
7 550 Tg O<sub>3</sub>/yr from Stevenson et al. (2006). We note that degrading the vertical resolution in the  
8 stratosphere (from 72 to 47 levels) does not impact the stratospheric source of ozone into the  
9 troposphere, suggesting that stratosphere-troposphere exchange (STE) is not influenced by the  
10 reduction in levels in the middle and upper stratosphere. Additional details of the configuration  
11 of the O<sub>3</sub> simulation in the version of GEOS-Chem used here are described in Zhang et al.  
12 (2011). The use of the GEOS-Chem 4D-var system for assimilation of ozone observations is  
13 described in Singh et al. (2011).

### 14 **3 Results and Discussion**

#### 15 **3.1 CO<sub>2</sub>/O<sub>3</sub> correlations in the Arctic**

16 Deng et al. (2014) compared the a posteriori CO<sub>2</sub> fields from their inversion analysis of the  
17 GOSAT data to HIPPO-3 data in the lower troposphere (between 1 – 5 km) and found that the  
18 mean differences between the model and the data were small, less than 0.20 ppm. In Fig. 2, we  
19 compare the a posteriori CO<sub>2</sub> fields (defined as our standard inversion here) with the HIPPO-3  
20 data in the upper troposphere (above 5 km). The linear correlation between the HIPPO-3  
21 observations and the modeled CO<sub>2</sub> is high, R<sup>2</sup>=0.7708, but there is a large bias at high latitudes  
22 in the northern hemisphere, where the observed CO<sub>2</sub> mixing ratio values are much lower than the  
23 modeled CO<sub>2</sub>. The HIPPO data are 10-second averages, and we are aware that at a temporal  
24 resolution of 10 seconds, the HIPPO data will reflect CO<sub>2</sub> on spatial scales that are much smaller  
25 than the model resolution. Consequently, representativeness errors associated with the coarse  
26 model grid and temporal resolution will contribute to the differences between the model and the  
27 data. Xiong et al. (2013) reported the occurrence of a strong stratospheric intrusion over North  
28 America on 27 March 2010, which was captured by the HIPPO data. They reported significantly  
29 reduced CH<sub>4</sub> values, reflecting stratospheric air that was transported down as low as 550 hPa,  
30 which would be consistent with the low CO<sub>2</sub> values of 385 ppm measured by HIPPO (in Fig. 2).

1 Because of the coarse horizontal resolution of the model simulation, it is possible that the model  
2 underestimates the stratospheric intrusion (e.g., Lin et al., 2012).

3 The influx of stratospheric air will be associated with low CO<sub>2</sub> and high O<sub>3</sub>; therefore, we  
4 examined the CO<sub>2</sub>/O<sub>3</sub> correlations in the HIPPO data and in the model. Tracer-tracer correlations  
5 have been used extensively to study transport and mixing in the stratosphere (e.g., Plumb and  
6 Ko, 1992; Waugh et al., 1997; Hoor et al., 2002; Sankey and Shepherd, 2003; Pan et al., 2004).  
7 The correlations, shown in Fig. 3, indicate a clear separation of tropospheric air (with low ozone  
8 and high CO<sub>2</sub>) and stratospheric air (with high ozone and low CO<sub>2</sub>), with a mixing region in  
9 between, with intermediate CO<sub>2</sub> and O<sub>3</sub> values that reflect the mixing between the tropospheric  
10 and stratospheric air masses. Shown also are linear fits to the HIPPO data in the stratospheric and  
11 mixing regions. Assuming an ozone threshold of 100 ppb as the transition from tropospheric air  
12 to stratospheric air (e.g., Pan et al., 2004), the intercept of the stratospheric branch with the 100  
13 ppb ozone threshold suggests a tropopause CO<sub>2</sub> level of about 387 ppm, in the absence of  
14 mixing. The modeled correlation agrees well with the data in the tropospheric and stratospheric  
15 branches, but the modeled values are displaced to higher CO<sub>2</sub> compared to the aircraft data in the  
16 mixing region, suggesting excessive mixing in the model (e.g., Hoor et al., 2002; Pan et al.,  
17 2004). We believe that the two clear mixing lines in Fig. 3 reflect the effects of the intrusion  
18 reported by Xiong et al. (2013), which the model does not capture. The mixing feature starting at  
19 CO<sub>2</sub> and O<sub>3</sub> abundances of 385 ppm and 400 ppb, respectively, corresponds to stratospheric air  
20 extending down to 7 - 8 km, while the feature starting at CO<sub>2</sub> and O<sub>3</sub> abundances of 386 ppm and  
21 300 ppb, respectively, extends down to 5-7 km. Although the model does not capture these  
22 features, the correlations suggest that the mean state of the model in the UTLS is characterized  
23 by stronger mixing than suggested by the observations.

24 Examination of the CO and O<sub>3</sub> correlations reveals a similar discrepancy, with the modeled CO  
25 and O<sub>3</sub> correlation shifted relative to the HIPPO data, as shown for CO<sub>2</sub> and O<sub>3</sub> in Fig. 3. The  
26 HIPPO CO/O<sub>3</sub> correlations also show the influence of the enhanced STE at O<sub>3</sub> values less than  
27 400 ppb, which is not captured by the model. We also examined the CO/O<sub>3</sub> and CO<sub>2</sub>/O<sub>3</sub>  
28 correlations in HIPPO-1 in January 2009 and found similar discrepancies between the model and  
29 the aircraft data. In a separate study, (MacKenzie et al., 2015) used ACE-FTS CO and O<sub>3</sub> data to  
30 evaluate the stratosphere-troposphere mixing layer in the GEOS-Chem model. They found that  
31 vertical extent of the mixing layer simulated by the model agrees with that derived from ACE-

1 FTS data. However, at high-latitudes the altitude of the mixing layer in the model is biased high  
2 relative to that from ACE-FTS, whereas at low-latitudes it is biased low.

3 Since CO<sub>2</sub> and O<sub>3</sub> are both long-lived tracers in the lower stratosphere, and their distributions  
4 largely reflect the influence of transport, we chose to optimize the modeled O<sub>3</sub> distribution and  
5 use the observed CO<sub>2</sub>/O<sub>3</sub> correlation to obtain an observation-based adjustment to the modeled  
6 CO<sub>2</sub> distribution. To improve the modeled ozone distribution, we assimilated OSIRIS ozone  
7 observations using the GEOS-Chem 4D-var system. The 4D-Var assimilation scheme adjusts the  
8 initial O<sub>3</sub> conditions to optimize the model trajectory over the assimilation window. If the  
9 window is long compared to the lifetime of ozone, the assimilation system is unable to use the  
10 information from observations toward the end of the window to adjust the initial conditions,  
11 since that information is chemically destroyed. On the other hand, if the window is too short,  
12 there is less data available to adjust the state. In the high-latitude UTLS, the O<sub>3</sub> lifetime is long,  
13 however, in the tropical middle troposphere, the O<sub>3</sub> lifetime is about three weeks (Wang et al.,  
14 1998). Consequently, we chose a two-week assimilation window, from March 20, 2010 to April  
15 2, 2010. Furthermore, since the Arctic HIPPO measurements were made on March 26th and 27<sup>th</sup>,  
16 we chose the assimilation window so that the timing of the HIPPO data would fall at the  
17 midpoint of the window, providing the best constraint on the O<sub>3</sub> distribution at that time.

18 The changes in the modeled O<sub>3</sub> fields as a result of the assimilation are shown in Fig. 4. The  
19 assimilation increased O<sub>3</sub> in the lowermost stratosphere by about 10-20% and decreased it by as  
20 much as 40% in the tropical and subtropical UTLS. To evaluate the modeled O<sub>3</sub> fields, we  
21 compared the a priori and a posteriori ozone fields with data from the ACE-FTS instrument,  
22 shown in Fig. 5. The modeled ozone distributions were sampled at the ACE-FTS observation  
23 locations and times (we selected the model grid box consistent with the location of the 30 km  
24 tangent height). The comparisons shown used 31 ACE-FTS profiles between 55°N – 65°N and  
25 44 profiles between 65°N- 75°N during the period March 20, 2010 to April 3, 2010. In the  
26 Arctic, between 100 – 20 hPa both the a priori and a posteriori ozone fields agree with the ACE-  
27 FTS data to within 10%. At these altitudes, the a priori bias was -2.7% between 55°N – 65°N  
28 (Fig. 5a), while the a posteriori bias was 1%. Between 65°N - 75°N, the a priori and a posteriori  
29 biases were 2.3% and 4.4%, respectively. At lower altitudes, the model bias was larger, with the  
30 a priori model underestimating ACE-FTS O<sub>3</sub> by as much as 30-40% near 200 hPa. The  
31 assimilation reduced the underestimate to within 15-25% of the ACE-FTS data. Despite this

1 large residual bias at these levels, the assimilated ozone fields represent a significant  
2 improvement over the a priori in the lower stratosphere. It should be noted that because the data  
3 from both OSIRIS and ACE-FTS are limb measurements, the information obtained from them is  
4 more limited at pressures of 200 hPa and higher.

5 With the optimized stratospheric O<sub>3</sub>, we used the empirical fit between CO<sub>2</sub> and O<sub>3</sub> from the  
6 HIPPO CO<sub>2</sub>/O<sub>3</sub> correlations to produce an adjustment to the modeled CO<sub>2</sub> in the lower  
7 stratosphere. Examination of CO<sub>2</sub>/O<sub>3</sub> correlations in the model at the locations of the HIPPO data  
8 and elsewhere across the modeled Arctic produced negligible differences in the correlations.  
9 Consequently, although the HIPPO measurements were localized over the Pacific (over Alaska  
10 on March 26 - 27, 2010), we applied the empirical fit throughout the Arctic to produce a zonal  
11 mean adjustment to the modeled CO<sub>2</sub> profile in the Arctic. The zonal mean change in the vertical  
12 profile of CO<sub>2</sub> in the Arctic as a result of the HIPPO-derived adjustment is shown in Fig. 6. The  
13 HIPPO CO<sub>2</sub>/O<sub>3</sub> correlations suggest a steeper vertical gradient in CO<sub>2</sub> across the tropopause,  
14 which is consistent with the results of MacKenzie et al. (2015) that showed that the stratosphere-  
15 troposphere mixing region in the model is biased high relative to the tropopause at high latitudes.  
16 We examined the CO<sub>2</sub>/O<sub>3</sub> correlation throughout the month of March 2010 found little variations  
17 in the correlations, so we applied the adjustment to the CO<sub>2</sub> vertical distribution throughout  
18 March. This adjustment was then imposed in the modeled CO<sub>2</sub> fields and we repeated the  
19 GOSAT inversion from Deng et al. (2014), but only for the growing season, March – August  
20 2010, to assess the impact of this perturbation in CO<sub>2</sub> in the Arctic UTLS on the inferred surface  
21 fluxes of CO<sub>2</sub>. This adjustment to the Arctic CO<sub>2</sub> distribution corresponds to a sink in the global  
22 mass of CO<sub>2</sub> of 0.6 Pg C in the GOSAT inversion analysis. Ideally, one would use seasonally  
23 varying CO<sub>2</sub>/O<sub>3</sub> correlations to obtain the appropriate UTLS CO<sub>2</sub> adjustment over the seasonal  
24 cycle. However, there was only one HIPPO campaign (in spring) in 2010. Consequently, as a  
25 first step in assessing the potential impact of this discrepancy in the UTLS on the flux estimates  
26 we chose to impose a constant adjustment to the CO<sub>2</sub> distribution. It should be noted that if the  
27 UTLS discrepancy is due to excessive vertical mixing then we would expect it to be larger when  
28 the vertical gradient in CO<sub>2</sub> is large. This means that we would expect the discrepancy to be  
29 present from March until summer, by July or August, when the summertime drawdown reverses  
30 the vertical gradient in CO<sub>2</sub> in the troposphere.

## 1 **3.2 Passive Tracer Experiments**

2 To help understand the potential impact of the adjustment to CO<sub>2</sub> in the Arctic UTLS shown in  
3 Fig. 6, we conducted forward sensitivity analyses using a passive CO<sub>2</sub>-like tracer in the model.  
4 As mentioned above, the Arctic UTLS adjustment leads a total atmospheric CO<sub>2</sub> mass decrease  
5 of 0.60 between March – August, 2010, so for the passive tracer experiment we imposed an  
6 equivalent source. This way, the source matches the change in CO<sub>2</sub> in the UTLS shown in Fig. 6.  
7 As in the inversion analysis, we impose the adjustment across the whole Arctic, but here it is a  
8 source, whereas it is sink in the inversion analysis. The zonal mean distribution of the passive  
9 tracer is shown in Fig. 7 for March and June 2010. Within the first month, there is significant  
10 transport of the stratospheric CO<sub>2</sub> down into the mid-latitude and subtropical troposphere. In  
11 summer, there is transport to the southern hemisphere in the tropical UTLS, as described by  
12 Miyazaki et al. (2008). By June the tracer has been transported south as far as 30°S (Fig. 7b), and  
13 by August, the tracer distribution extends as far as 60°S (not shown).

14 In Fig. 8 we have plotted the distribution of the tracer in terms of the column averaged dry mole  
15 fraction (XCO<sub>2</sub>). We have sampled the tracer distribution at the GOSAT observation locations  
16 and times and applied the GOSAT averaging kernels to smooth the tracer in a manner that is  
17 consistent with the vertical sensitivity of the GOSAT retrievals. Although the imposed source is  
18 located mainly in the stratosphere, its impact on the CO<sub>2</sub> column, as reflected in the XCO<sub>2</sub>  
19 values, is not negligible. By June, the perturbation in XCO<sub>2</sub> exceeds 0.5 ppm in the mid- and  
20 high-latitudes of the northern hemisphere. As a result of the inter-hemispheric transport in the  
21 tropical UTLS, we see small corrections of about 0.1 – 0.2 ppm in XCO<sub>2</sub> in the southern tropics  
22 and subtropics. In June, the XCO<sub>2</sub> changes are confined to equatorward of 30°S, reflecting the  
23 southern extent of the tracer transport in the upper troposphere (Fig. 7b). However, by August,  
24 the influence of the Arctic source is reflected in the XCO<sub>2</sub> values across all of South America  
25 and Australia. We note that even though the tracer is accumulating in the troposphere over the  
26 course of the run, the impact on XCO<sub>2</sub> in the southern hemisphere in August is still small, about  
27 0.1 – 0.2 ppm. The results in Fig. 8 are interesting, nevertheless, as they demonstrate that the  
28 perturbations in CO<sub>2</sub> in the UTLS can have a noticeable impact on XCO<sub>2</sub> values, which have  
29 implications for interpreting differences in inversion analyses using XCO<sub>2</sub> and in situ surface  
30 data.

### 1 3.3 Inversion Analyses

2 Using the inversion approach of Deng et al. (2014), we assimilated the ACOS GOSAT XCO<sub>2</sub>  
3 from March 1 – August 31, 2010, with the reduction in UTLS CO<sub>2</sub> in the Arctic. Shown in Fig. 9  
4 are the inversion results, aggregated to the TransCom regions. Without the Arctic UTLS  
5 adjustment, we obtained an estimated land sink of CO<sub>2</sub> of -6.65 Pg C for March – August 2010.  
6 With the imposed reduction in the CO<sub>2</sub> in the Arctic, the estimated land sink was reduced to -  
7 5.71 Pg C. The largest absolute changes in the regional flux estimates were obtained for  
8 temperate North America (from -1.34 Pg C to -1.08 Pg C) and Europe (from -1.55 Pg to -1.36 Pg  
9 C). The flux estimate for the other regions, such as Boreal North America, Boreal Eurasia,  
10 temperate Eurasia, and tropical Asia, all changed by about 0.1 Pg C. As a relative change, the  
11 difference in the flux estimate for tropical Asia was large, with the flux decreasing by a factor of  
12 two from -0.26 Pg C to -0.13 Pg C. In the rest of the tropics, the largest change was for tropical  
13 South America, for which the flux estimate increased 23%, from 0.19 to 0.23 Pg C. The flux  
14 estimate for Northern Africa increased from 0.01 Pg C to 0.06 Pg C.

15 Deng et al. (2014) showed that the GOSAT data suggest that the bottom-up biospheric fluxes  
16 used in this version of GEOS-Chem underestimate the summertime sinks of CO<sub>2</sub>. For example,  
17 their GOSAT-derived estimate for the June sink of CO<sub>2</sub> for temperate North America was -0.5  
18 Pg C compared their a priori of about -0.3 Pg C. Since, as shown in Fig. 6, much of the  
19 perturbation in CO<sub>2</sub> in the Arctic UTLS is transported down in the troposphere, the imposed  
20 reduction in UTLS CO<sub>2</sub> during the growing season requires weaker surface sinks to bring the  
21 model into agreement with the GOSAT data. In the experiment here, the largest changes are  
22 obtained for the mid-latitude flux regions in North America and Europe, due to transport of the  
23 lower stratospheric adjustment down, along the isentropes (shown in Fig. 4), into the middle and  
24 upper troposphere of the mid-latitudes and subtropics. We believe that the large change obtained  
25 for the tropical Asian flux may be due to the influence of STE associated with the Asian  
26 monsoon (e.g. Postel and Hitchman, 1999; Shuckburgh et al., 2009).

27 In general, the inversion results show that reducing the CO<sub>2</sub> mixing ratio in the Arctic UTLS  
28 decreased the sinks in most northern land regions and increased the sources in the tropics. As  
29 mentioned above, the decreased northern land sinks are due to the fact that the imposed UTLS  
30 sink compensates for the summertime uptake at the surface. We believe that the increased

1 tropical sources are due to the fact that the UTLS sink exacerbates the underestimate of CO<sub>2</sub> in  
2 the model in the tropical upper troposphere. Fig. 2 shows that there is a residual negative bias in  
3 CO<sub>2</sub>, relative to the HIPPO data, in the upper troposphere in the northern tropics and subtropics  
4 in the standard inversion. As shown by the transport pattern in Fig. 7b, the imposed reduction in  
5 the UTLS CO<sub>2</sub> will exacerbate this bias, forcing the inversion to compensate by increasing the  
6 tropical sources. This underestimate in tropical CO<sub>2</sub> is consistent with the argument that the  
7 lowermost stratospheric bias shown in Figs. 3 and 6 is due to excessive mixing across the  
8 tropopause in the subtropics. Excessive STE would result in enhanced CO<sub>2</sub> (and reduced O<sub>3</sub>) in  
9 the extratropical lowermost stratosphere and reduced CO<sub>2</sub> (and enhanced O<sub>3</sub>) in the tropical  
10 upper troposphere. Indeed, assimilation of the OSIRIS data, as shown in Fig. 4, increased ozone  
11 in the extratropical lowermost stratosphere and decreased it in the upper tropical troposphere.  
12 Consequently, the imposed reduction in CO<sub>2</sub> in the Arctic UTLS should be accompanied by an  
13 increase in CO<sub>2</sub> in the tropical and subtropical upper troposphere.

14 Unlike the extratropical UTLS, use of the CO<sub>2</sub>/O<sub>3</sub> correlations in the tropical UTLS to adjust the  
15 CO<sub>2</sub> distribution is challenging because of the effects of convective transport and the chemical  
16 production of O<sub>3</sub> on the tracer-tracer relationship in the tropical upper troposphere. Therefore, as  
17 a first step, we chose to impose a uniform source of CO<sub>2</sub> of about 0.25 ppm between 8°N - 20°N  
18 and about 5 – 8 km, to remove the mean bias between the model and the HIPPO CO<sub>2</sub> data in this  
19 region. This constant 0.25 ppm adjustment corresponds to a total source of 0.55 Pg C for March  
20 – August 2010, and almost balances the imposed Arctic sink. The inversion results with the  
21 combined UTLS sink in the Arctic and the tropical source are shown in Figs. 9 and 10. The  
22 global land sink was estimated as -6.64 Pg C with the combined Arctic sink and tropical source,  
23 a 0.01 Pg C difference from -6.65 Pg C obtained in the standard inversion. The flux estimates for  
24 three most northern land regions were relatively unchanged with the tropical adjustment. Europe,  
25 for example, was estimated as a sink of -1.39 Pg C with the combined source and the sink  
26 compared to -1.36 Pg C with just the Arctic sink. While small changes were obtained from  
27 northern temperate regions. Temperate North America, for example, was inferred as a sink of -  
28 1.22 Pg C with the combined Arctic and tropical adjustments compared to -1.08 Pg C with just  
29 the Arctic adjustment. Although the global land sink with the Arctic and tropical adjustment was  
30 consistent with that estimated in the standard inversion, we found that the total northern land sink  
31 (for March – August) was 0.98 Pg C weaker with the Arctic and tropical adjustment than in the

1 standard inversion. This large latitudinal change in the land sink is due to the fact that a stronger  
2 extratropical drawdown during the growing season is required to account for the high latitude  
3 UTLS bias in the standard inversion.

4 As expected, the largest relative differences with the addition of the tropical source were for the  
5 tropical regions. For tropical South America, the flux estimate increased by 23% with only the  
6 Arctic sink, whereas it was reduced by 77% with the combined Arctic sink and tropical source.  
7 For Northern Africa, where the fluxes are small for March - August, the flux estimates changed  
8 sign, going from 0.06 Pg C with the Arctic sink to -0.13 Pg C with the combined Arctic sink and  
9 tropical source. With only the Arctic sink, we found that the flux estimate for tropical Asia was  
10 reduced by a factor of two. However, the addition of the tropical source compensated for the  
11 influence of the Arctic sink on this region, producing a flux estimate of -0.30 Pg C, which is a  
12 slightly stronger sink than that inferred in the standard inversion (-0.26 Pg C). Despite the  
13 apparent consistency between the tropical Asian flux estimates from the standard inversion and  
14 from the inversion with the combined source and sink, the transition from being a source to a  
15 sink for CO<sub>2</sub> is impacted by the specification of the tropical source. The standard inversion  
16 suggested a weak source for March, which shifted to a sink in April. However, the inversion with  
17 the combined source and sink produced a weak sink in March, which became a weak source in  
18 April, before strongly transitioning to a sink in June.

### 19 **3.4 Impact of Model Resolution**

20 To assess the potential impact of model resolution, we doubled the model resolution to 2° x 2.5°  
21 and repeated the forward model simulation from 1 July 2009 to 31 December 2010. Because of  
22 the large number of iterations required for minimizing the cost function, it is computationally  
23 expensive to carry out the global inversion analysis at the 2° x 2.5° resolution. As a result, we  
24 focus here on a comparison of the forward model simulation. Shown in Fig. 11 is the zonal mean  
25 vertical profile of CO<sub>2</sub> at 75°N on 1 April 2010. The model configuration used to produce the  
26 results in Fig. 11 is similar to, but not identical to that used for the results in Figs. 1-3 and Fig. 6.  
27 Here we use the a posteriori scaling factors (the ratio of the a posteriori to a priori fluxes) from  
28 the standard CO<sub>2</sub> inversion to scale the fossil fuel, biofuel, ocean, and biospheric CO<sub>2</sub> fluxes, but  
29 the biomass burning emissions are not scaled. As shown in Fig. 11, the higher resolution  
30 simulation produced a steeper gradient in CO<sub>2</sub> than the low-resolution simulation, which is



1 consistent with excessive vertical mixing in the  $4^\circ \times 5^\circ$  simulation. Examination of the latitudinal  
2 distribution in the UTLS, shown in Fig. 12 reveals more  $\text{CO}_2$  in the upper tropical and  
3 subtropical troposphere and less  $\text{CO}_2$  in the high latitude lower stratosphere in the  $2^\circ \times 2.5^\circ$  run  
4 compared to the  $4^\circ \times 5^\circ$  run; the latitudinal gradient in the northern hemisphere UTLS is weaker  
5 in the low resolution simulation.

6 In Table 1 we have listed the mean differences between the standard a posteriori  $\text{CO}_2$  and the  
7 HIPPO data above 8 km, binned into four latitudinal bins. As discussed above, the largest biases  
8 are in the polar region, with a positive bias of 1.72 ppm between  $60^\circ - 90^\circ\text{N}$ . In the lower  
9 latitudes the model is biased low, with a bias of -0.09 ppm between  $0^\circ - 15^\circ\text{N}$  and -0.31 ppm  
10 between  $15^\circ - 45^\circ\text{N}$ . Also listed in Table 1 are mean differences between the  $4^\circ \times 5^\circ$  and  $2^\circ \times$   
11  $2.5^\circ$  simulations. Between  $60^\circ - 90^\circ\text{N}$  the low resolution simulation is higher by 0.55 ppm,  
12 which is almost a third of the high bias between the low resolution simulation and the HIPPO  
13 data. In the tropics ( $0^\circ - 15^\circ\text{N}$ ), the difference between the  $4^\circ \times 5^\circ$  and  $2^\circ \times 2.5^\circ$  simulations is  
14 equivalent to the differences between the  $4^\circ \times 5^\circ$  simulation and the HIPPO data.

15

## 16 **4 Conclusions**

17 We have evaluated the GEOS-Chem  $\text{CO}_2$  simulation in the extratropical UTLS using aircraft  
18 observations from the HIPPO-3 campaign in March 2010 and found that the model overestimates  
19  $\text{CO}_2$  in the lowermost stratosphere in the Arctic. Comparison of the modeled and observed  
20 correlations between  $\text{CO}_2$  and  $\text{O}_3$ , suggest a discrepancy in mixing in the UTLS in the model. To  
21 obtain an observation-based adjustment to  $\text{CO}_2$  in the model, we assimilated  $\text{O}_3$  data from the  
22 OSIRIS instrument to improve the stratospheric  $\text{O}_3$  in the model and then used the assimilated  $\text{O}_3$   
23 together with the HIPPO  $\text{CO}_2/\text{O}_3$  correlation to infer an adjustment to the modeled  $\text{CO}_2$  in the  
24 Arctic. The HIPPO-based adjustment to the modeled  $\text{CO}_2$  resulted in an increase in the vertical  
25 gradient in  $\text{CO}_2$  across the Arctic tropopause.

26 To assess the potential impact of these changes in  $\text{CO}_2$  on regional  $\text{CO}_2$  flux estimates, we  
27 conducted inversion analyses using GOSAT  $\text{XCO}_2$  data, with and without the  $\text{CO}_2$  adjustment in  
28 the Arctic UTLS. Because of the lack of data to evaluate the  $\text{CO}_2/\text{O}_3$  correlations over the  
29 seasonal cycle, the adjustment in the Arctic UTLS was assumed to be constant over the  
30 assimilation period, from March – August 2010, representing a total sink of 0.60 Pg C in the

1 Arctic UTLS. We found that this adjustment in Arctic CO<sub>2</sub> resulted in a reduction in the inferred  
2 flux of CO<sub>2</sub> from temperate North America and Europe during the growing season of 19% and  
3 13% respectively, compared to the standard inversion (without the sink). For tropical Asia, there  
4 was a factor of two reduction in the estimated flux.

5 If the bias in CO<sub>2</sub> reflects the influence of excessive STE, one would expect the overestimate in  
6 CO<sub>2</sub> in the extratropical lower stratosphere to be accompanied by an overestimate in CO<sub>2</sub> in the  
7 tropical and subtropical upper troposphere. Indeed, we find that the modeled CO<sub>2</sub> is biased low  
8 relative to the HIPPO data in these regions. Also, relative to the OSIRIS data, the modeled O<sub>3</sub> is  
9 biased low in the extratropical lower stratosphere and high in the tropical and subtropical upper  
10 troposphere, which is consistent with excessive STE. We conducted a sensitivity experiment in  
11 which we corrected the underestimate in CO<sub>2</sub> in the low-latitude upper troposphere by imposing  
12 a uniform source of CO<sub>2</sub> of 0.55 Pg C (an adjustment of 0.25 ppm) for March – August 2010 in  
13 the tropical upper troposphere to remove the mean difference between the HIPPO data and the a  
14 posteriori CO<sub>2</sub> from the standard GOSAT inversion. With the extratropical sink and tropical  
15 source in the UTLS, the CO<sub>2</sub> source inferred from tropical South America was reduced by 77%.  
16 In contrast, with only the Arctic sink it was increased by 23%. For tropical Asia, the total  
17 estimated flux with extratropical sink and tropical source in the UTLS was close to the estimate  
18 in the standard inversion. Although the imposed sources and sinks were ad hoc, due to the lack  
19 of data to better quantify the evolution of the model errors over the seasonal cycle, the results  
20 here illustrate that discrepancies in the CO<sub>2</sub> distribution in the UTLS can impact the regional  
21 CO<sub>2</sub> flux estimates using satellite data, and point to the need to better characterize model errors  
22 in the UTLS.

23 Inversion analyses using GOSAT XCO<sub>2</sub> data tend to produce stronger sinks in the extratropical  
24 northern hemisphere and weaker sources in the tropics compared to those using the surface flask  
25 data (Houweling et al., 2015). In our analysis we found that with the combined Arctic and  
26 tropical adjustment, the March – August sink in northern lands was 0.98 Pg C weaker than in our  
27 standard inversion, even though the estimated total global sink in the two inversions were  
28 similar. Our results suggest that the high latitude UTLS discrepancy could result in a latitudinal  
29 redistribution of mass in flux inversions, and we would expect the XCO<sub>2</sub> inversions to be more  
30 sensitive to the UTLS discrepancies than the flask inversions.

1 As we noted in the introduction, the CO<sub>2</sub> distribution in the extratropical UTLS in winter and  
2 spring represents a balance between a positive tendency associated with large-scale eddies and a  
3 negative tendency due to the transport by the mean meridional circulation (Miyazaki et al.,  
4 2008). The meridional circulation is, in part, driven by the large-scale eddies, and the balance  
5 between the two tendency terms will vary from model to model. It is possible that the inability of  
6 GEOS-Chem to reproduce the HIPPO CO<sub>2</sub>/O<sub>3</sub> correlations in the extratropical UTLS may be due  
7 to discrepancies in either the large-scale eddies or the meridional circulation in the model. On the  
8 one hand, GEOS-Chem is driven by assimilated meteorological fields, so it is expected that the  
9 model will capture the large-scale eddies well. On the other hand, it is known that CTMs, which  
10 are driven by reanalyses, capture vertical transport in the UTLS less well than free running  
11 general circulation models because the data assimilation systems introduce imbalance between  
12 the temperature and wind fields (Douglass et al., 2003). It is because of this that CTMs generally  
13 underestimate the mean age of air in the stratosphere.

14 Other potential sources of discrepancy in the CO<sub>2</sub> distribution are the numerical scheme used in  
15 the model and the resolution of the model simulation. Prather et al. (2008) compared the CO<sub>2</sub>  
16 simulations from two CTMs using the same meteorological fields and CO<sub>2</sub> fluxes, but with  
17 different numerical schemes. One model, the Global Modeling Initiative (GMI) CTM, used the  
18 numerical transport scheme by Lin and Rood (1996), whereas the other model, the University of  
19 California, Irvine (UCI) CTM, used the Second-Order Moments (SOM) scheme by Prather  
20 (1986). At a resolution of 5° x 4°, the GMI model, with the Lin and Rood (1996) scheme, was  
21 more diffusive, producing a weaker seasonal cycle in CO<sub>2</sub> and higher CO<sub>2</sub> values in the  
22 stratosphere. Prather et al. (2008) found that doubling the resolution of the models to 2° x 2.5°  
23 reduced the discrepancies, but the GMI model still had numerical errors that were twice as large  
24 as those in the UCI model. We found that doubling our model resolution to 2° x 2.5° increased  
25 the vertical gradient in CO<sub>2</sub> in the high latitudes, and reduced the CO<sub>2</sub> loading in the high-  
26 latitude lower stratosphere. The 4° x 5° simulation overestimated the Arctic CO<sub>2</sub> (averaged 60° –  
27 90°N and above 8 km) by 0.55 ppm, relative to the 2° x 2.5° simulation which is almost a third  
28 of the high bias between the low-resolution simulation and the HIPPO data. In the tropics (0° -  
29 15°N), the difference between the 4° x 5° and 2° x 2.5° simulations is equivalent to the  
30 differences between the 4° x 5° simulation and the HIPPO data. In contrast, the 4° x 5° was  
31 biased low by 0.23 ppm relative to the 2° x 2.5° simulation between 15° – 45°N, which is

1 equivalent to the differences between the  $4^\circ \times 5^\circ$  simulation and the HIPPO data, suggesting that  
2 the mixing is excessive in the low-resolution simulation.

3 There has been a number of studies looking at the impact of transport discrepancies in the UTLS  
4 on the distribution of  $O_3$  and other long-lived tracers, using aircraft, balloon, and satellite  
5 observations (e.g., Considine et al., 2008; Strahan and Polansky, 2006).  
6 But additional attention is needed to understand the impact of these discrepancies in the context  
7 of  $CO_2$  flux inversions. We expect that the discrepancies identified here will be more of an issue  
8 for inversion analyses using satellite data than those using surface data, since all thermal infrared  
9 and shortwave infrared, nadir satellite retrievals have sensitivity to  $CO_2$  in the UTLS. Based on  
10 our results, it is unclear the degree to which further increases in the spatial resolution of the  
11 model simulation will mitigate the biases in the UTLS. Additional studies using GEOS-Chem at  
12 higher spatial resolution, such as at the native resolution of  $0.5^\circ \times 0.67^\circ$  would be helpful. Also,  
13 additional data are needed to better evaluate the model performance in the UTLS. High-  
14 resolution  $CO_2$  profile measurements across the UTLS would be useful. Simultaneous satellite  
15 measurements of  $CO_2$ ,  $O_3$  and other long-lived tracers from instruments such as limb sounders,  
16 would enable us to better exploit tracer-tracer correlations to evaluate model transport in the  
17 UTLS in the context of the  $CO_2$  flux inversions. For example,  $CO_2$  vertical profiles have also  
18 been retrieved from ACE-FTS (Sioris et al., 2014); however the data are currently sparse due to  
19 the initial cloud filtering method used, and thus were not used in the current work. Efforts are  
20 underway to retrieve profiles down to cloud tops, so that fewer profiles are lost, which could aid  
21 in future analyses.

22

### 23 **Acknowledgements**

24 This work was funded by the Canadian Space Agency (CSA), the Natural Sciences and  
25 Engineering Research Council of Canada (NSERC), and the NASA Atmospheric  $CO_2$   
26 Observations from Space (ACOS) program (grant number NNX10AT42G). The GOSAT data  
27 were produced by the ACOS/OCO-2 project at the Jet Propulsion Laboratory, California Institute  
28 of Technology, and obtained from the ACOS/OCO-2 data archive maintained at the NASA  
29 Goddard Earth Science Data and Information Services Center. The Atmospheric Chemistry  
30 Experiment (ACE) is a Canadian-led mission mainly supported by the CSA and NSERC. Odin is

1 a Swedish-led satellite project funded jointly by Sweden (SNSB), Canada (CSA), France  
2 (CNES), and Finland (Tekes). We thank the two anonymous reviewers for helpful comments on  
3 the manuscript.

4

5

## 6 **References**

7

8 Adams, C., Bourassa, A. E., Bathgate, A. F., McLinden, C. A., Lloyd, N. D., Roth, C. Z.,  
9 Llewellyn, E. J., Zawodny, J. M., Flittner, D. E., Manney, G. L., Daffer, W. H., and Degenstein,  
10 D. A.: Characterization of Odin-OSIRIS ozone profiles with the SAGE II dataset, *Atmos. Meas.*  
11 *Tech.*, 6, 1447-1459, 10.5194/amt-6-1447-2013, 2013.

12 Andres, R. J., Gregg, J. S., Losey, L., Marland, G., and Boden, T. A.: Monthly, global emissions  
13 of carbon dioxide from fossil fuel consumption, *Tellus B*, 63, 309-327, 10.1111/j.1600-  
14 0889.2011.00530.x, 2011.

15 Basu, S., Guerlet, S., Butz, A., Houweling, S., Hasekamp, O., Aben, I., Krummel, P., Steele, P.,  
16 Langenfelds, R., Torn, M., Biraud, S., Stephens, B., Andrews, A., and Worthy, D.: Global CO<sub>2</sub>  
17 fluxes estimated from GOSAT retrievals of total column CO<sub>2</sub>, *Atmospheric Chemistry and*  
18 *Physics*, 13, 8695-8717, 10.5194/acp-13-8695-2013, 2013.

19 Bernath, P. F., McElroy, C. T., Abrams, M. C., Boone, C. D., Butler, M., Camy-Peyret, C.,  
20 Carleer, M., Clerbaux, C., Coheur, P. F., Colin, R., DeCola, P., DeMazière, M., Drummond, J.  
21 R., Dufour, D., Evans, W. F. J., Fast, H., Fussen, D., Gilbert, K., Jennings, D. E., Llewellyn, E.  
22 J., Lowe, R. P., Mahieu, E., McConnell, J. C., McHugh, M., McLeod, S. D., Michaud, R.,  
23 Midwinter, C., Nassar, R., Nichitiu, F., Nowlan, C., Rinsland, C. P., Rochon, Y. J., Rowlands,  
24 N., Semeniuk, K., Simon, P., Skelton, R., Sloan, J. J., Soucy, M. A., Strong, K., Tremblay, P.,  
25 Turnbull, D., Walker, K. A., Walkty, I., Wardle, D. A., Wehrle, V., Zander, R., and Zou, J.:  
26 Atmospheric Chemistry Experiment (ACE): Mission overview, *Geophysical Research Letters*,  
27 32, L15S01, 10.1029/2005gl022386, 2005.

28 Boone, C. D., Nassar, R., Walker, K. A., Rochon, Y., McLeod, S. D., Rinsland, C. P., and  
29 Bernath, P. F.: Retrievals for the atmospheric chemistry experiment Fourier-transform  
30 spectrometer, *Applied Optics*, 44, 7218-7231, 10.1364/ao.44.007218, 2005.

31 Bourassa, A. E., McLinden, C. A., Bathgate, A. F., Elash, B. J., and Degenstein, D. A.: Precision  
32 estimate for Odin-OSIRIS limb scatter retrievals, *Journal of Geophysical Research*, 117,  
33 10.1029/2011jd016976, 2012.

34 Chen, J. M., Liu, J., Cihlar, J., and Goulden, M. L.: Daily canopy photosynthesis model through  
35 temporal and spatial scaling for remote sensing applications, *Ecological Modelling*, 124, 99-119,  
36 1999.

37 Chevallier, F., Palmer, P. I., Feng, L., Boesch, H., O'Dell, C. W., and Bousquet, P.: Toward  
38 robust and consistent regional CO<sub>2</sub> flux estimates from in situ and spaceborne measurements of

1 atmospheric CO<sub>2</sub>, *Geophysical Research Letters*, 41, 2013GL058772, 10.1002/2013gl058772,  
2 2014.

3 Considine, D. B., Logan, J. A., and Olsen, M. A.: Evaluation of near-tropopause ozone  
4 distributions in the Global Modeling Initiative combined stratosphere/troposphere model with  
5 ozonesonde data, *Atmos. Chem. Phys.*, 8, 2365-2385, 10.5194/acp-8-2365-2008, 2008.

6 Corbett, J. J., and Koehler, H. W.: Updated emissions from ocean shipping, *J. Geophys. Res.*,  
7 108, 4650-4666, 10.1029/2003jd003751, 2003.

8 Corbett, J. J.: Considering alternative input parameters in an activity-based ship fuel  
9 consumption and emissions model: Reply to comment by Øyvind Endresen et al. on "Updated  
10 emissions from ocean shipping", *Journal of Geophysical Research*, 109, 10.1029/2004jd005030,  
11 2004.

12 Degenstein, D. A., Bourassa, A. E., Roth, C. Z., and Llewellyn, E. J.: Limb scatter ozone  
13 retrieval from 10 to 60 km using a multiplicative algebraic reconstruction technique, *Atmos.*  
14 *Chem. Phys.*, 9, 6521-6529, 10.5194/acp-9-6521-2009, 2009.

15 Deng, F., Chen, J. M., Plummer, S., Chen, M., and Pisek, J.: Algorithm for global leaf area index  
16 retrieval using satellite imagery, *IEEE Transactions on Geoscience and Remote Sensing*, 44,  
17 2219-2229, 10.1109/tgrs.2006.872100, 2006.

18 Deng, F., and Chen, J. M.: Recent global CO<sub>2</sub> flux inferred from atmospheric CO<sub>2</sub> observations  
19 and its regional analyses, *Biogeosciences*, 8, 3263-3281, 10.5194/bg-8-3263-2011, 2011.

20 Deng, F., Jones, D. B. A., Henze, D. K., Bousserez, N., Bowman, K. W., Fisher, J. B., Nassar,  
21 R., O'Dell, C., Wunch, D., Wennberg, P. O., Kort, E. A., Wofsy, S. C., Blumenstock, T.,  
22 Deutscher, N. M., Griffith, D. W. T., Hase, F., Heikkinen, P., Sherlock, V., Strong, K.,  
23 Sussmann, R., and Warneke, T.: Inferring regional sources and sinks of atmospheric CO<sub>2</sub> from  
24 GOSAT XCO<sub>2</sub> data, *Atmospheric Chemistry and Physics*, 14, 3703-3727, 10.5194/acp-14-3703-  
25 2014, 2014.

26 Douglass, A. R., Schoeberl, M. R., Rood, R. B., and Pawson, S.: Evaluation of transport in the  
27 lower tropical stratosphere in a global chemistry and transport model, *Journal of Geophysical*  
28 *Research: Atmospheres*, 108, 4259, 10.1029/2002jd002696, 2003.

29 Endresen, Ø., Sørsgård, E., Bakke, J., and Isaksen, I. S. A.: Substantiation of a lower estimate for  
30 the bunker inventory: Comment on "Updated emissions from ocean shipping" by James J.  
31 Corbett and Horst W. Koehler, *J. Geophys. Res.*, 109, D23302, 10.1029/2004jd004853, 2004.

32 Endresen, Ø., Sørsgård, E., Behrens, H. L., Brett, P. O., and Isaksen, I. S. A.: A historical  
33 reconstruction of ships' fuel consumption and emissions, *J. Geophys. Res.*, 112, D12301,  
34 10.1029/2006jd007630, 2007.

35 Friedl, R. R.: Atmospheric effects of subsonic aircraft: interim assessment report of the  
36 Advanced Subsonic Technology Program, in, National Aeronautics and Space Administration,  
37 Goddard Space Flight Center, Greenbelt, MD United States, 168, 1997.

38 Hegglin, M. I., Boone, C. D., Manney, G. L., Shepherd, T. G., Walker, K. A., Bernath, P. F.,  
39 Daffer, W. H., Hoor, P., and Schiller, C.: Validation of ACE-FTS satellite data in the upper  
40 troposphere/lower stratosphere (UTLS) using non-coincident measurements, *Atmos. Chem.*  
41 *Phys.*, 8, 1483-1499, 10.5194/acp-8-1483-2008, 2008.

1 Henze, D. K., Hakami, A., and Seinfeld, J. H.: Development of the adjoint of GEOS-Chem,  
2 Atmos. Chem. Phys., 7, 2413-2433, 10.5194/acp-7-2413-2007, 2007.

3 Hoor, P., Fischer, H., Lange, L., Lelieveld, J., and Brunner, D.: Seasonal variations of a mixing  
4 layer in the lowermost stratosphere as identified by the CO-O<sub>3</sub> correlation from in situ  
5 measurements, Journal of Geophysical Research: Atmospheres, 107, ACL 1-1-ACL 1-11,  
6 10.1029/2000jd000289, 2002.

7 Houweling, S., Baker, D., Basu, S., Boesch, H., Butz, A., Chevallier, F., Deng, F., Dlugokencky,  
8 E. J., Feng, L., Ganshin, A., Hasekamp, O., Jones, D., Maksyutov, S., Marshall, J., Oda, T.,  
9 O'Dell, C. W., Oshchepkov, S., Palmer, P. I., Peylin, P., Poussi, Z., Reum, F., Takagi, H.,  
10 Yoshida, Y., and Zhuravlev, R.: An intercomparison of inverse models for estimating sources  
11 and sinks of CO<sub>2</sub> using GOSAT measurements, Journal of Geophysical Research: Atmospheres,  
12 n/a-n/a, 10.1002/2014jd022962, 2015.

13 Kalnay, E., Kanamitsu, M., Kistler, R., Collins, W., Deaven, D., Gandin, L., Iredell, M., Saha,  
14 S., White, G., Woollen, J., Zhu, Y., Leetmaa, A., Reynolds, R., Chelliah, M., Ebisuzaki, W.,  
15 Higgins, W., Janowiak, J., Mo, K. C., Ropelewski, C., Wang, J., Jenne, R., and Joseph, D.: The  
16 NCEP/NCAR 40-Year Reanalysis Project, Bulletin of the American Meteorological Society, 77,  
17 437-471, 10.1175/1520-0477(1996)077<0437:TNYRP>2.0.CO;2, 1996.

18 Kim, B. Y., Fleming, G. G., Lee, J. J., Waitz, I. A., Clarke, J.-P., Balasubramanian, S., Malwitz,  
19 A., Klima, K., Locke, M., Holsclaw, C. A., Maurice, L. Q., and Gupta, M. L.: System for  
20 assessing Aviation's Global Emissions (SAGE), Part 1: Model description and inventory results,  
21 Transportation Research Part D: Transport and Environment, 12, 325-346,  
22 10.1016/j.trd.2007.03.007, 2007.

23 Lauvaux, T., and Davis, K. J.: Planetary boundary layer errors in mesoscale inversions of  
24 column-integrated CO<sub>2</sub> measurements, Journal of Geophysical Research: Atmospheres, 119,  
25 490-508, 10.1002/2013jd020175, 2014.

26 Lin, M., Fiore, A. M., Cooper, O. R., Horowitz, L. W., Langford, A. O., Levy, H., Johnson, B. J.,  
27 Naik, V., Oltmans, S. J., and Senff, C. J.: Springtime high surface ozone events over the western  
28 United States: Quantifying the role of stratospheric intrusions, Journal of Geophysical Research:  
29 Atmospheres, 117, n/a-n/a, 10.1029/2012jd018151, 2012.

30 Lin, S.-J., and Rood, R. B.: Multidimensional Flux-Form Semi-Lagrangian Transport Schemes,  
31 Monthly Weather Review, 124, 2046-2070, 10.1175/1520-  
32 0493(1996)124<2046:mffslt>2.0.co;2, 1996.

33 Llewellyn, E. J., Lloyd, N. D., Degenstein, D. A., Gattinger, R. L., Petelina, S. V., Bourassa, A.  
34 E., Wiensz, J. T., Ivanov, E. V., McDade, I. C., Solheim, B. H., McConnell, J. C., Haley, C. S.,  
35 von Savigny, C., Sioris, C. E., McLinden, C. A., Griffioen, E., Kaminski, J., Evans, W. F.,  
36 Puckrin, E., Strong, K., Wehrle, V., Hum, R. H., Kendall, D. J., Matsushita, J., Murtagh, D. P.,  
37 Brohede, S., Stegman, J., Witt, G., Barnes, G., Payne, W. F., Piché, L., Smith, K., Warshaw, G.,  
38 Deslauniers, D. L., Marchand, P., Richardson, E. H., King, R. A., Wevers, I., McCreath, W.,  
39 Kyrölä, E., Oikarinen, L., Leppelmeier, G. W., Auvinen, H., Mégie, G., Hauchecorne, A.,  
40 Lefèvre, F., de La Nöe, J., Ricaud, P., Frisk, U., Sjöberg, F., von Schéele, F., and Nordh, L.: The  
41 OSIRIS instrument on the Odin spacecraft, Canadian Journal of Physics, 82, 411-422,  
42 10.1139/p04-005, 2004.

1 MacKenzie, D., Jones, D. B. A., Hegglin, M., Boone, C. D., Walker, K. A., Bernath, P. F., and  
2 Murray, L.: Global Structure of the UTLS Mixing Layer and its Link to Regional Stratosphere–  
3 Troposphere Exchange, in preparation, 2015.

4 Maksyutov, S., Takagi, H., Valsala, V. K., Saito, M., Oda, T., Saeki, T., Belikov, D. A., Saito,  
5 R., Ito, A., Yoshida, Y., Morino, I., Uchino, O., Andres, R. J., and Yokota, T.: Regional CO<sub>2</sub> flux  
6 estimates for 2009–2010 based on GOSAT and ground-based CO<sub>2</sub> observations, *Atmospheric  
7 Chemistry and Physics*, 13, 9351-9373, 10.5194/acp-13-9351-2013, 2013.

8 McLinden, C. A., Olsen, S. C., Hannegan, B., Wild, O., Prather, M. J., and Sundet, J.:  
9 Stratospheric ozone in 3-D models: A simple chemistry and the cross-tropopause flux, *Journal of  
10 Geophysical Research: Atmospheres*, 105, 14653-14665, 10.1029/2000jd900124, 2000.

11 Miyazaki, K., Patra, P. K., Takigawa, M., Iwasaki, T., and Nakazawa, T.: Global-scale transport  
12 of carbon dioxide in the troposphere, *Journal of Geophysical Research*, 113,  
13 10.1029/2007jd009557, 2008.

14 Nassar, R., Jones, D. B. A., Suntharalingam, P., Chen, J. M., Andres, R. J., Wecht, K. J.,  
15 Yantosca, R. M., Kulawik, S. S., Bowman, K. W., Worden, J. R., Machida, T., and Matsueda,  
16 H.: Modeling global atmospheric CO<sub>2</sub> with improved emission inventories and CO<sub>2</sub> production  
17 from the oxidation of other carbon species, *Geoscientific Model Development*, 3, 689-716,  
18 10.5194/gmd-3-689-2010, 2010.

19 O'Dell, C. W., Connor, B., Bösch, H., O'Brien, D., Frankenberg, C., Castano, R., Christi, M.,  
20 Eldering, D., Fisher, B., Gunson, M., McDuffie, J., Miller, C. E., Natraj, V., Oyafuso, F.,  
21 Polonsky, I., Smyth, M., Taylor, T., Toon, G. C., Wennberg, P. O., and Wunch, D.: The ACOS  
22 CO<sub>2</sub> retrieval algorithm – Part 1: Description and validation against synthetic observations,  
23 *Atmospheric Measurement Techniques*, 5, 99-121, 10.5194/amt-5-99-2012, 2012.

24 Pan, L. L., Randel, W. J., Gary, B. L., Mahoney, M. J., and Hints, E. J.: Definitions and  
25 sharpness of the extratropical tropopause: A trace gas perspective, *Journal of Geophysical  
26 Research: Atmospheres*, 109, D23103, 10.1029/2004jd004982, 2004.

27 Parazoo, N. C., Denning, A. S., Kawa, S. R., Pawson, S., and Lokupitiya, R.: CO<sub>2</sub> flux  
28 estimation errors associated with moist atmospheric processes, *Atmospheric Chemistry and  
29 Physics*, 12, 6405-6416, 10.5194/acp-12-6405-2012, 2012.

30 Plumb, R. A., and Ko, M. K. W.: Interrelationships between mixing ratios of long-lived  
31 stratospheric constituents, *Journal of Geophysical Research: Atmospheres*, 97, 10145-10156,  
32 10.1029/92jd00450, 1992.

33 Postel, G. A., and Hitchman, M. H.: A Climatology of Rossby Wave Breaking along the  
34 Subtropical Tropopause, *Journal of the Atmospheric Sciences*, 56, 359-373, 10.1175/1520-  
35 0469(1999)056<0359:acorwb>2.0.co;2, 1999.

36 Prather, M. J.: Numerical advection by conservation of second-order moments, *Journal of  
37 Geophysical Research: Atmospheres*, 91, 6671-6681, 10.1029/JD091iD06p06671, 1986.

38 Prather, M. J., Zhu, X., Strahan, S. E., Steenrod, S. D., and Rodriguez, J. M.: Quantifying errors  
39 in trace species transport modeling, *Proc Natl Acad Sci U S A*, 105, 19617-19621,  
40 10.1073/pnas.0806541106, 2008.



1 Reuter, M., Buchwitz, M., Hilker, M., Heymann, J., Schneising, O., Pillai, D., Bovensmann, H.,  
2 Burrows, J. P., Bösch, H., Parker, R., Butz, A., Hasekamp, O., O'Dell, C. W., Yoshida, Y.,  
3 Gerbig, C., Nehrkorn, T., Deutscher, N. M., Warneke, T., Notholt, J., Hase, F., Kivi, R.,  
4 Sussmann, R., Machida, T., Matsueda, H., and Sawa, Y.: Satellite-inferred European carbon sink  
5 larger than expected, *Atmos. Chem. Phys.*, 14, 13739–13753, 10.5194/acp-14-13739-2014,  
6 2014.

7 Sankey, D., and Shepherd, T. G.: Correlations of long-lived chemical species in a middle  
8 atmosphere general circulation model, *Journal of Geophysical Research: Atmospheres*, 108,  
9 4494, 10.1029/2002jd002799, 2003.

10 Shuckburgh, E., d'Ovidio, F., and Legras, B.: Local Mixing Events in the Upper Troposphere  
11 and Lower Stratosphere. Part II: Seasonal and Interannual Variability, *Journal of the*  
12 *Atmospheric Sciences*, 66, 3695-3706, 10.1175/2009jas2983.1, 2009.

13 Singh, K., Sandu, A., Bowman, K. W., Parrington, M., Jones, D. B. A., and Lee, M.: Ozone data  
14 assimilation with GEOS-Chem: a comparison between 3-D-Var, 4-D-Var, and suboptimal  
15 Kalman filter approaches, *Atmos. Chem. Phys. Discuss.*, 11, 22247-22300, 10.5194/acpd-11-  
16 22247-2011, 2011.

17 Stephens, B. B., Gurney, K. R., Tans, P. P., Sweeney, C., Peters, W., Bruhwiler, L., Ciais, P.,  
18 Ramonet, M., Bousquet, P., Nakazawa, T., Aoki, S., Machida, T., Inoue, G., Vinnichenko, N.,  
19 Lloyd, J., Jordan, A., Heimann, M., Shibistova, O., Langenfelds, R. L., Steele, L. P., Francey, R.  
20 J., and Denning, A. S.: Weak Northern and Strong Tropical Land Carbon Uptake from Vertical  
21 Profiles of Atmospheric CO<sub>2</sub>, *Science*, 316, 1732-1735, 10.1126/science.1137004, 2007.

22 Strahan, S. E., and Polansky, B. C.: Meteorological implementation issues in chemistry and  
23 transport models, *Atmos. Chem. Phys.*, 6, 2895-2910, 10.5194/acp-6-2895-2006, 2006.

24 Takahashi, T., Sutherland, S. C., Wanninkhof, R., Sweeney, C., Feely, R. A., Chipman, D. W.,  
25 Hales, B., Friederich, G., Chavez, F., Sabine, C., Watson, A., Bakker, D. C. E., Schuster, U.,  
26 Metzl, N., Yoshikawa-Inoue, H., Ishii, M., Midorikawa, T., Nojiri, Y., Körtzinger, A., Steinhoff,  
27 T., Hoppema, M., Olafsson, J., Arnarson, T. S., Tilbrook, B., Johannessen, T., Olsen, A.,  
28 Bellerby, R., Wong, C. S., Delille, B., Bates, N. R., and de Baar, H. J. W.: Climatological mean  
29 and decadal change in surface ocean pCO<sub>2</sub>, and net sea-air CO<sub>2</sub> flux over the global oceans,  
30 *Deep Sea Research Part II: Topical Studies in Oceanography*, 56, 554-577, 2009.

31 van der Werf, G. R., Randerson, J. T., Giglio, L., Collatz, G. J., Mu, M., Kasibhatla, P. S.,  
32 Morton, D. C., DeFries, R. S., Jin, Y., and van Leeuwen, T. T.: Global fire emissions and the  
33 contribution of deforestation, savanna, forest, agricultural, and peat fires (1997–2009), *Atmos.*  
34 *Chem. Phys.*, 10, 11707-11735, 10.5194/acp-10-11707-2010, 2010.

35 Wang, Y., Jacob, D. J., and Logan, J. A.: Global simulation of tropospheric O<sub>3</sub>-NO<sub>x</sub>-  
36 hydrocarbon chemistry: 3. Origin of tropospheric ozone and effects of nonmethane  
37 hydrocarbons, *Journal of Geophysical Research: Atmospheres*, 103, 10757-10767,  
38 10.1029/98jd00156, 1998.

39 Waugh, D. W., Plumb, R. A., Elkins, J. W., Fahey, D. W., Boering, K. A., Dutton, G. S., Volk,  
40 C. M., Keim, E., Gao, R. S., Daube, B. C., Wofsy, S. C., Loewenstein, M., Podolske, J. R., Chan,  
41 K. R., Proffitt, M. H., Kelly, K. K., Newman, P. A., and Lait, L. R.: Mixing of polar vortex air  
42 into middle latitudes as revealed by tracer-tracer scatterplots, *Journal of Geophysical Research:*  
43 *Atmospheres*, 102, 13119-13134, 10.1029/96jd03715, 1997.

1 Wilkerson, J. T., Jacobson, M. Z., Malwitz, A., Balasubramanian, S., Wayson, R., Fleming, G.,  
2 Naiman, A. D., and Lele, S. K.: Analysis of emission data from global commercial aviation:  
3 2004 and 2006, *Atmospheric Chemistry and Physics*, 10, 6391-6408, 10.5194/acp-10-6391-  
4 2010, 2010.

5 Wofsy, S. C., Team, H. S., Cooperating, M., and Satellite, T.: HIAPER Pole-to-Pole  
6 Observations (HIPPO): fine-grained, global-scale measurements of climatically important  
7 atmospheric gases and aerosols, *Philosophical transactions. Series A, Mathematical, physical,*  
8 *and engineering sciences*, 369, 2073-2086, 10.1098/rsta.2010.0313, 2011.

9 Wofsy, S. C., Daube, B. C., Jimenez, R., Kort, E., Pittman, J. V., Park, S., Commane, R., Xiang,  
10 B., Santoni, G., Jacob, D., Fisher, J., Pickett-Heaps, C., Wang, H., Wecht, K., Wang, Q.-Q.,  
11 Stephens, B. B., Shertz, S., Watt, A. S., Romashkin, P., Campos, T., Haggerty, J., Cooper, W. A.,  
12 Rogers, D., Beaton, S., Hendershot, R., Elkins, J. W., Fahey, D. W., Gao, R. S., Moore, F.,  
13 Montzka, S. A., Schwarz, J. P., Perring, A. E., Hurst, D., Miller, B. R., Sweeney, C., Oltmans, S.,  
14 Nance, D., Hintsa, E., Dutton, G., Watts, L. A., Spackman, J. R., Rosenlof, K. H., Ray, E. A.,  
15 Hall, B., Zondlo, M. A., Diao, M., Keeling, R., Bent, J., Atlas, E. L., Lueb, R., and Mahoney, M.  
16 J.: HIPPO Merged 10-second Meteorology, Atmospheric Chemistry, Aerosol Data  
17 (R\_20121129). Carbon Dioxide Information Analysis Center, Oak Ridge National Laboratory,  
18 Oak Ridge, Tennessee, USA, 10.3334/CDIAC/hippo\_010, 2012.

19 Xiong, X., Barnet, C., Maddy, E., Wofsy, S. C., Chen, L., Karion, A., and Sweeney, C.:  
20 Detection of methane depletion associated with stratospheric intrusion by atmospheric infrared  
21 sounder (AIRS), *Geophysical Research Letters*, 40, 2455-2459, 10.1002/grl.50476, 2013.

22 Yevich, R., and Logan, J. A.: An assessment of biofuel use and burning of agricultural waste in  
23 the developing world, *Global Biogeochem. Cycles*, 17, 1095-1134, 10.1029/2002gb001952,  
24 2003.

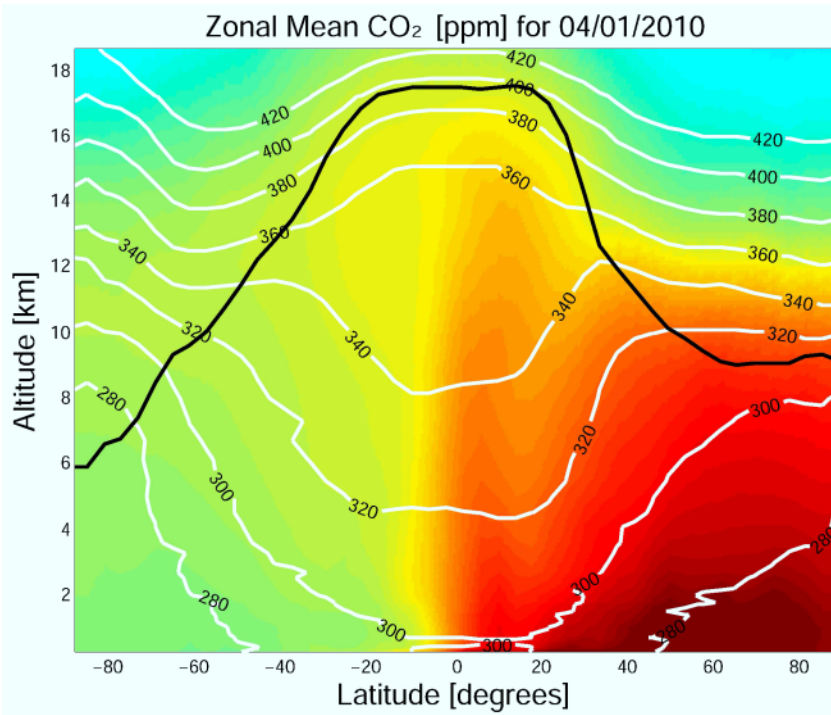
25 Zhang, L., Jacob, D. J., Downey, N. V., Wood, D. A., Blewitt, D., Carouge, C. C., van  
26 Donkelaar, A., Jones, D. B. A., Murray, L. T., and Wang, Y.: Improved estimate of the policy-  
27 relevant background ozone in the United States using the GEOS-Chem global model with  
28  $1/2^\circ \times 2/3^\circ$  horizontal resolution over North America, *Atmospheric Environment*, 45, 6769-6776,  
29 10.1016/j.atmosenv.2011.07.054, 2011.

30  
31  
32  
33  
34  
35  
36

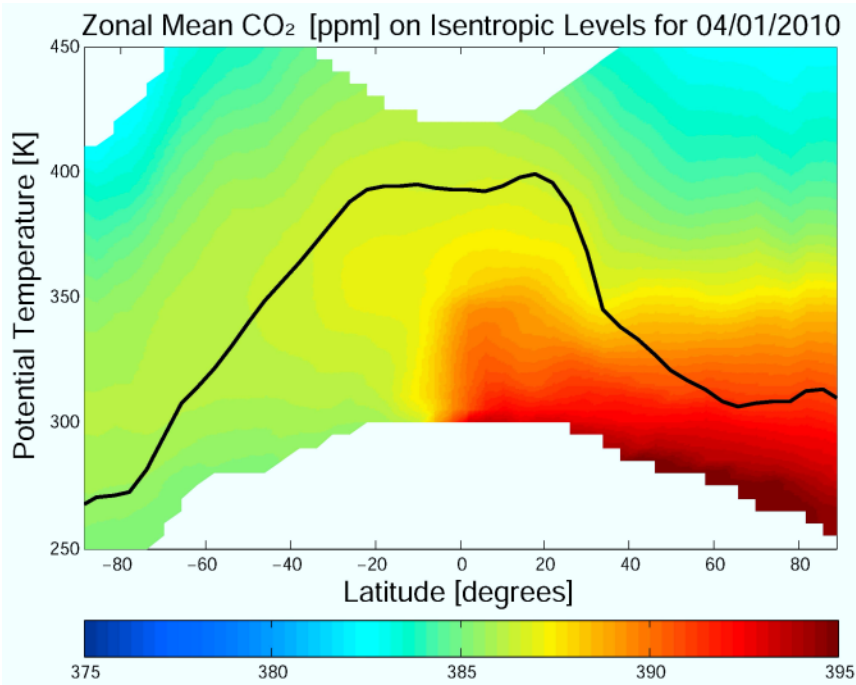
1  
2  
3  
4  
5  
6  
7  
8  
9  
10  
11  
12  
13  
14  
15

Table 1. Mean differences in CO<sub>2</sub> (ppm) between GEOS-Chem and HIPPO and between the GEOS-Chem 4° x 5° and 2° x 2.5° simulations.

GEOS-Chem - HIPPO Observation				GEOS-Chem 4x5 - GEOS-Chem 2x2.5			
0-15N	15-45N	45-60N	60-90N	0-15N	15-45N	45-60N	60-90N
-0.09	-0.31	1.60	1.72	-0.09	-0.23	-0.25	0.55
-0.23		1.68		-0.18		0.29	



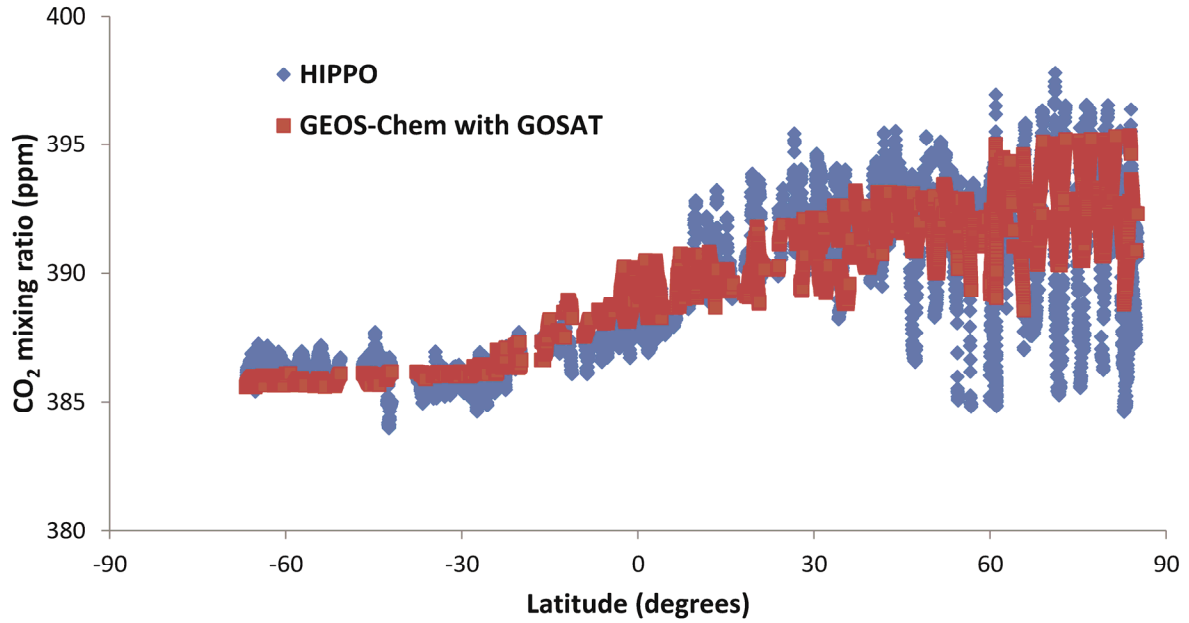
1



2

3 **Figure 1.** Zonal mean CO<sub>2</sub> from GEOS-Chem on April 1, 2010, as a function of latitude and  
 4 altitude (top) and latitude and potential temperature (bottom). In the latitude/altitude plot (top),  
 5 the white lines indicate the zonal mean potential temperature in Kelvins (K). The thick black line  
 6 in both plots denotes the location of the tropopause in the model.

1  
2



3

4 **Figure 2.** Comparison of modeled a posteriori CO<sub>2</sub> mixing ratios in the upper troposphere from  
5 our GOSAT inversion analysis (in red) with HIPPO observations (in blue) between 70°S to 84°N  
6 and above 5000 m in altitude. These a posteriori CO<sub>2</sub> fields are from the inversion denoted as our  
7 standard inversion.

8

9

10

11

12

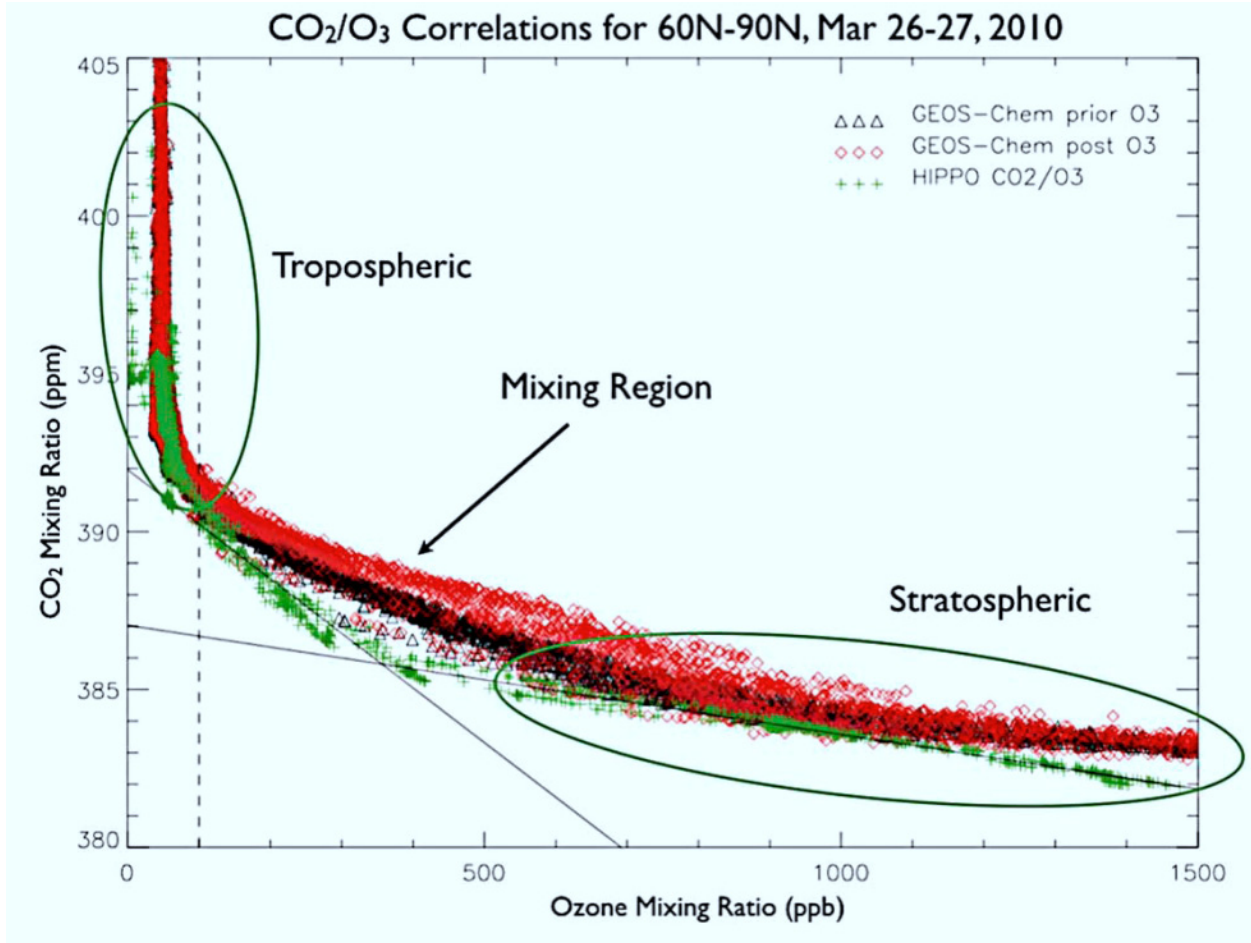
13

14

1

2

3

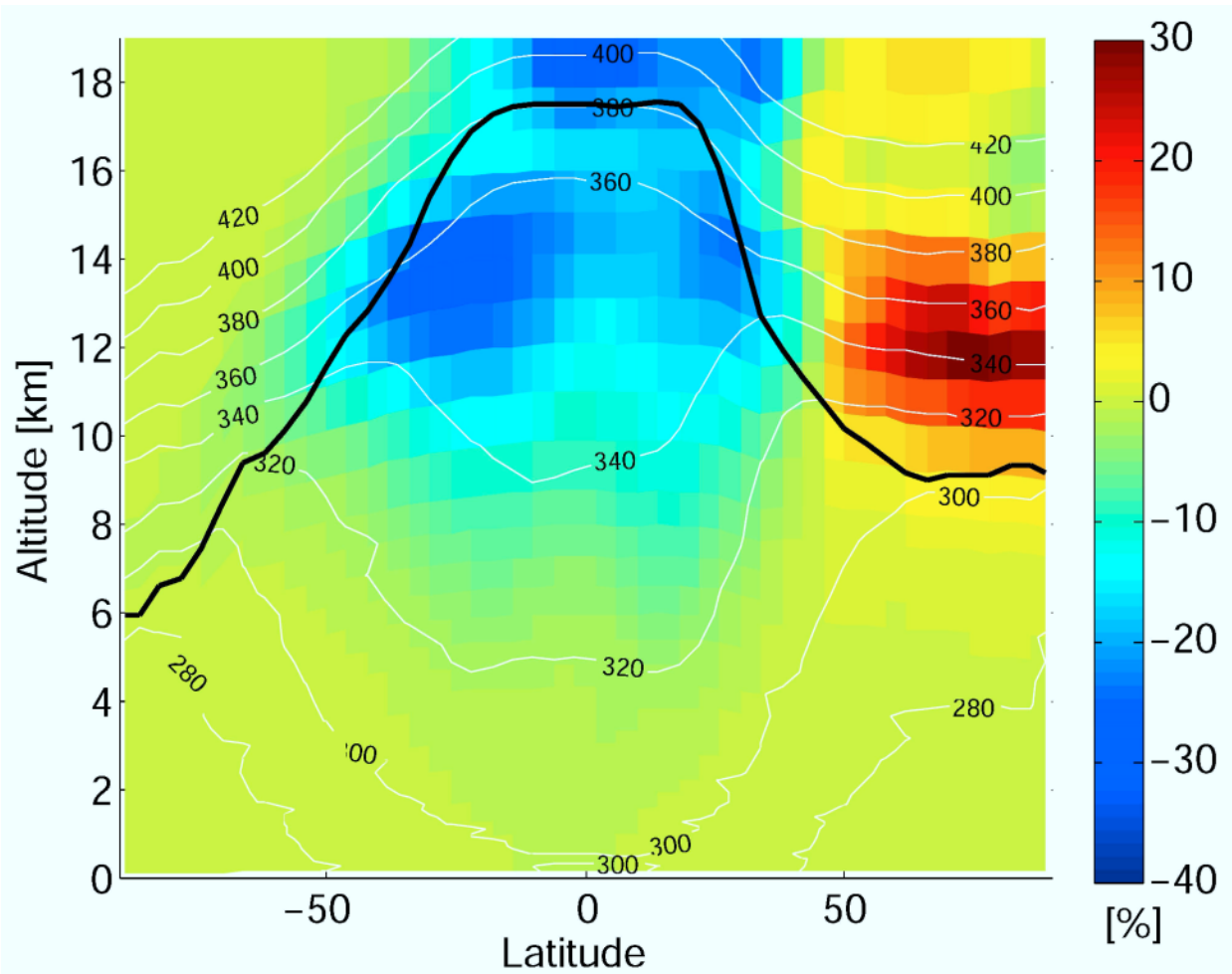


4

5 **Figure 3.** CO<sub>2</sub>/O<sub>3</sub> correlations from GEOS-Chem (red) and HIPPO-3 (green) for March 26-27,  
6 2010, poleward of 60°N. The high O<sub>3</sub> and low CO<sub>2</sub> values are characteristic of stratospheric air,  
7 whereas the low O<sub>3</sub> and high CO<sub>2</sub> values indicate tropospheric air. The values in the UTLS  
8 represent a mixture of stratospheric and tropospheric air. The red diamonds represent the GEOS-  
9 Chem CO<sub>2</sub>/O<sub>3</sub> correlations obtained after assimilation of the OSIRIS O<sub>3</sub> data in the stratosphere.  
10 The two thin black lines show the fit to the HIPPO data in the stratospheric branch and in the  
11 mixing region. The vertical dashed line indicates the 100 ppb threshold for O<sub>3</sub>, below which the  
12 air is considered tropospheric in origin.

13

1



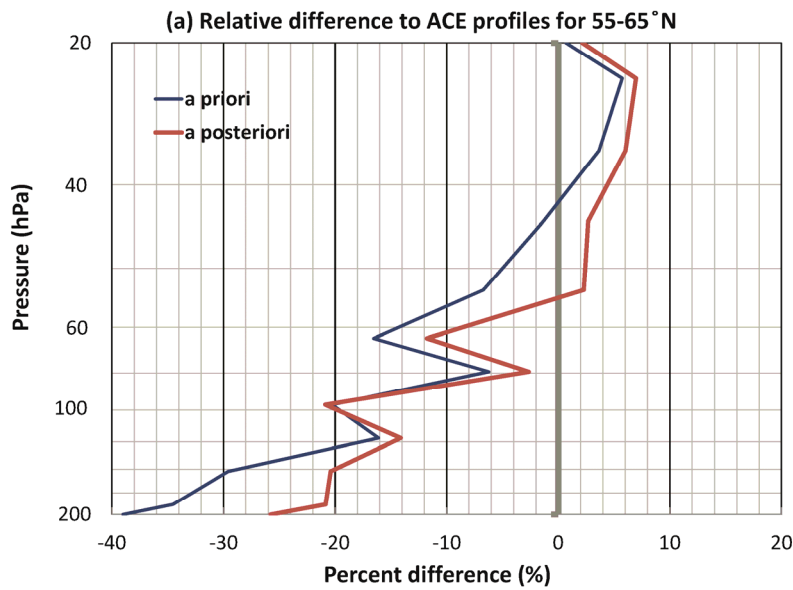
2

3 **Figure 4.** Zonal mean change in the GEOS-Chem O<sub>3</sub> distribution as a result of the assimilation  
4 of OSIRIS O<sub>3</sub> data. The assimilation was conducted for March 20 – April 2, 2010. As in Fig. 1,  
5 the white lines indicate the zonal mean potential temperature in Kelvins (K) and the thick black  
6 line denotes the location of the tropopause in the model.

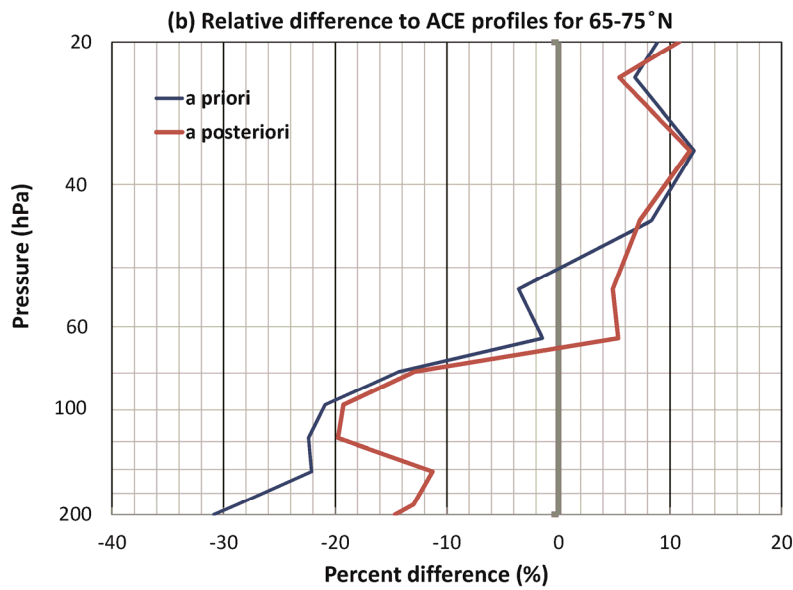
7

8

9



1



2

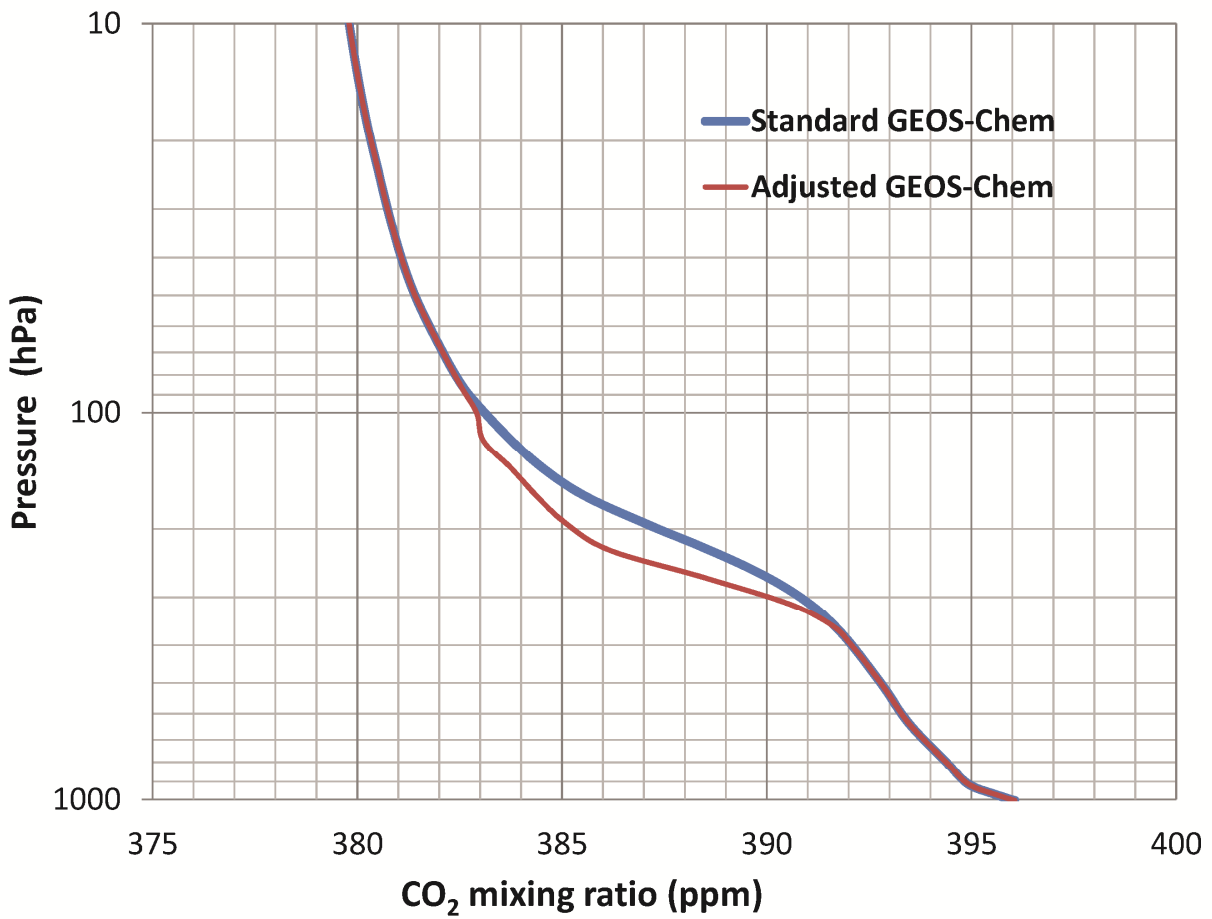
3 **Figure 5.** Relative difference between the a priori and a posteriori modeled O<sub>3</sub> and ACE-FTS O<sub>3</sub>  
 4 data. Shown are the mean differences for latitudes between 55°-65°N (a) and between 65°-75°N  
 5 (b).

6

7

8





1

2 **Figure 6.** The mean profile of CO<sub>2</sub> in the Arctic before (dashed line) and after (solid line) the  
 3 adjustment in in CO<sub>2</sub> in the UTLS based on the HIPPO-3 CO<sub>2</sub>/O<sub>3</sub> correlations.

4

5

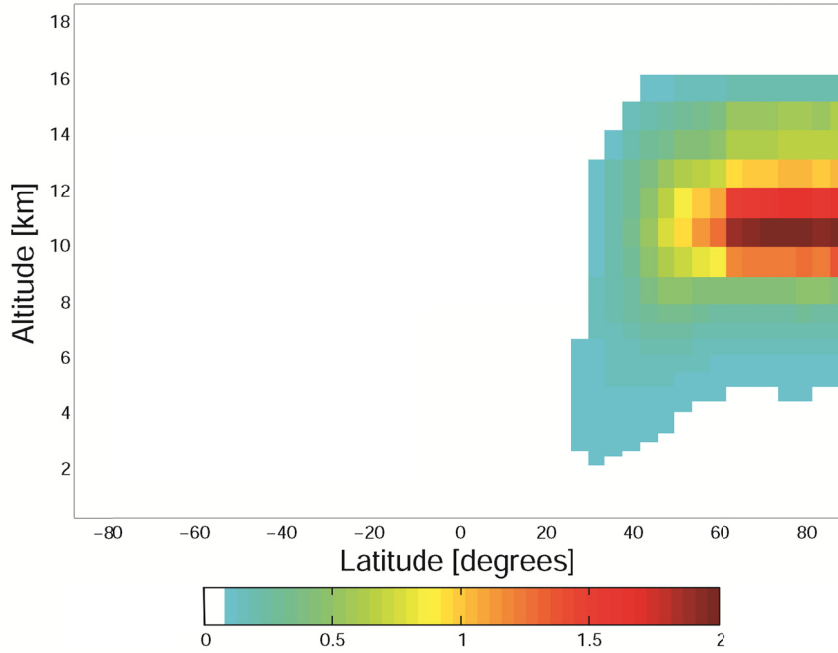
6

7

8

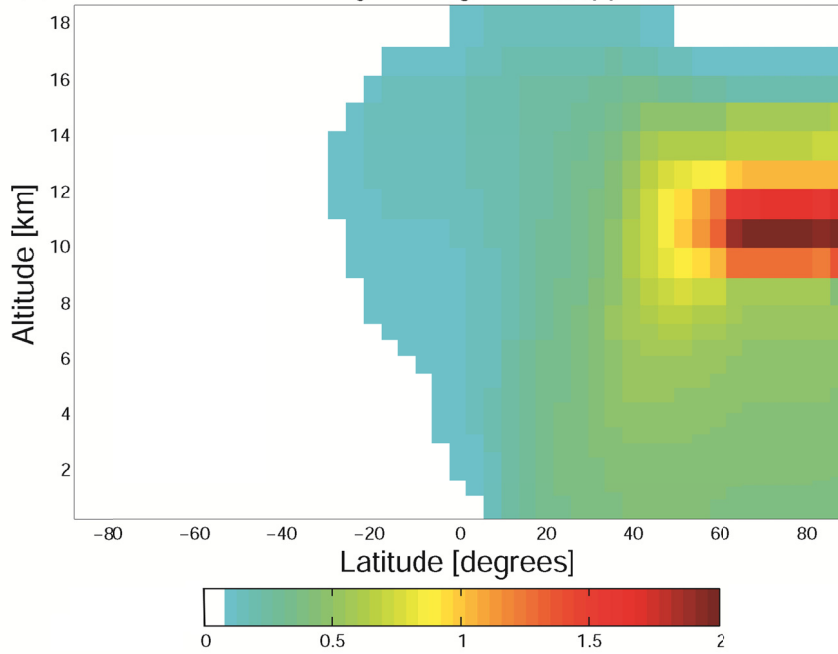
9

(a) Zonal Mean of Monthly Averaged CO<sub>2</sub> [ppm] for March 2010



1

(b) Zonal Mean of Monthly Averaged CO<sub>2</sub> [ppm] for June 2010

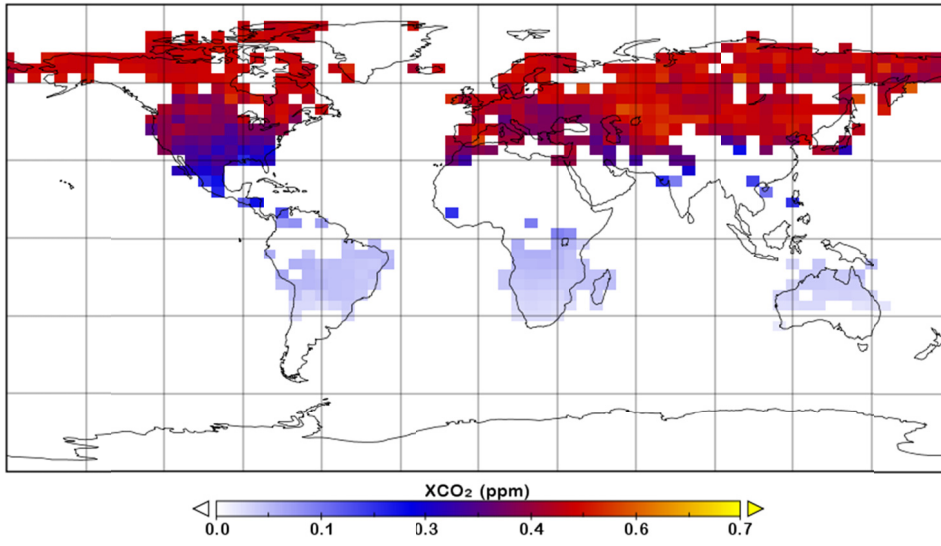


2

3 **Figure 7.** Monthly averaged, zonal mean distribution of a passive tracer with a constant source  
4 equivalent to the CO<sub>2</sub> adjustment in the Arctic UTLS for March – August 2010.

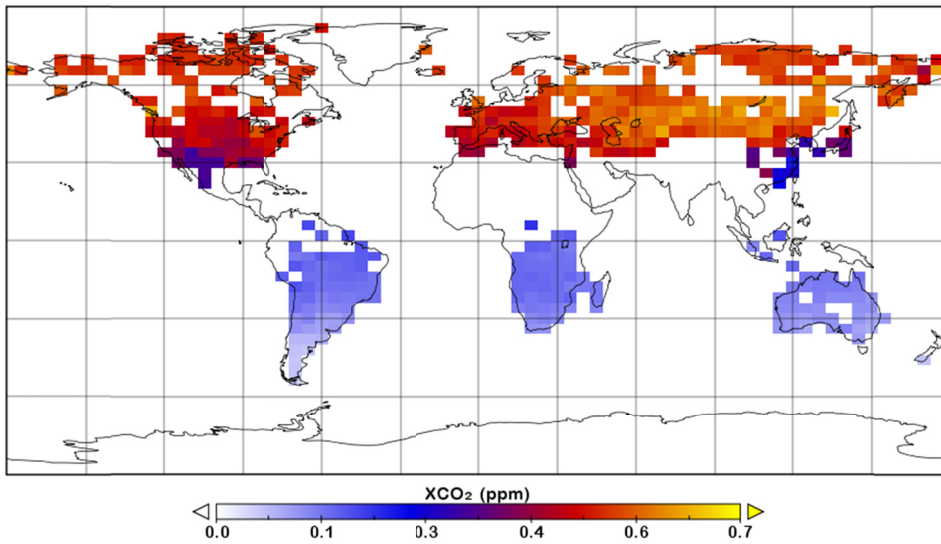
5

(a) Passive tracer XCO<sub>2</sub> for June 2010



1

(b) Passive tracer XCO<sub>2</sub> for August 2010



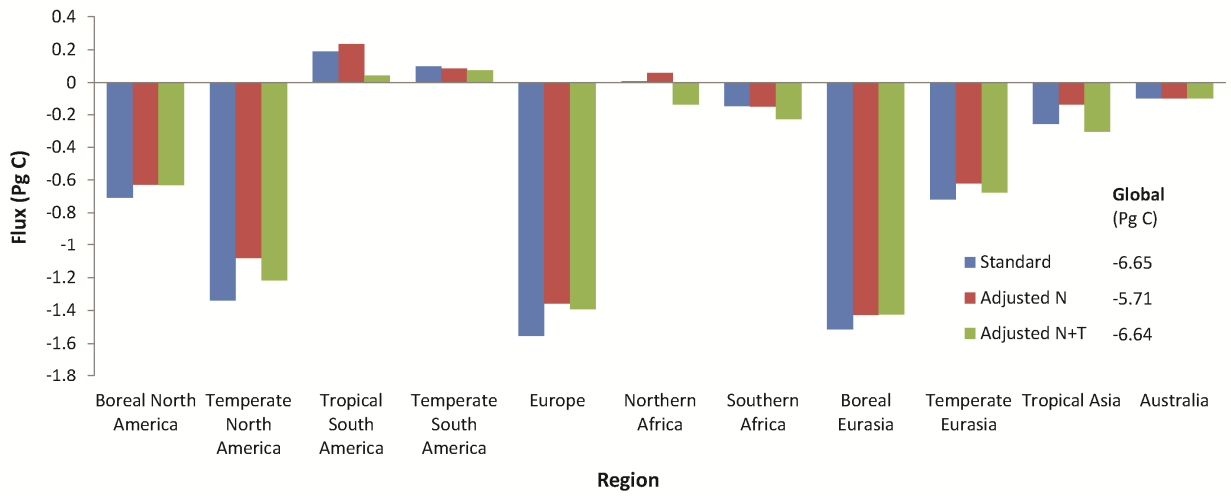
2

3 **Figure 8.** Monthly mean distribution of a passive tracer with a constant source equivalent to the  
4 CO<sub>2</sub> adjustment in the Arctic UTLS for March – August 2010. The tracer distribution was  
5 sampled at the GOSAT observation locations and times and vertically integrated, using the  
6 GOSAT averaging kernels, to produce XCO<sub>2</sub> values.

7

8

1



2

3 **Figure 9.** Regional CO<sub>2</sub> flux estimates for March to August 2010 inferred from GOSAT XCO<sub>2</sub>  
4 using the standard inversion approach (denoted Standard), with an imposed sink in CO<sub>2</sub> in the  
5 Arctic UTLS (denoted Adjusted N), and with the addition of uniform source in the upper  
6 troposphere in the northern tropics (denoted Adjusted N+T).

7

8

9

10

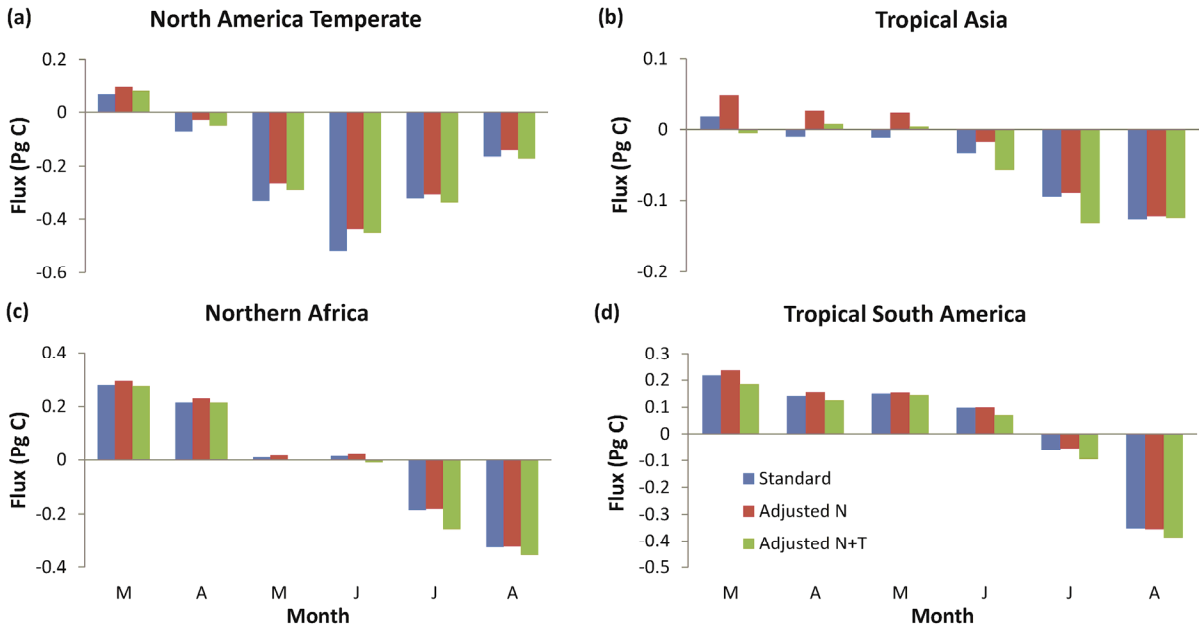
11

12

13

14

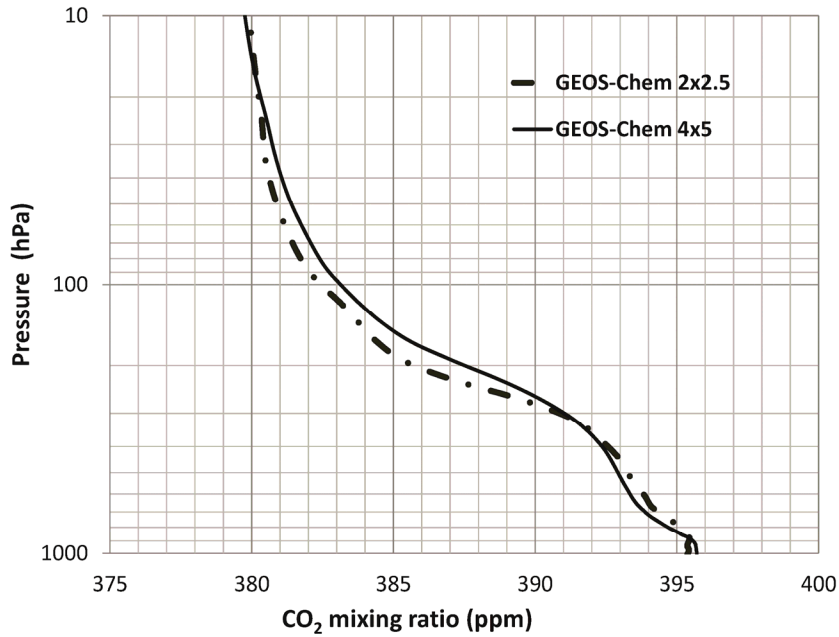
15



1  
2 **Figure 10.** Monthly mean CO<sub>2</sub> flux estimates for (a) Temperate North America, (b) Tropical  
3 Asia, (c) Northern Africa, and (d) Tropical South America. As in Fig. 9, shown are the results  
4 from using the standard inversion (denoted Standard)), with an imposed sink in CO<sub>2</sub> in the Arctic  
5 UTLS (denoted Adjusted N), and with the addition of uniform source in the upper troposphere in  
6 the northern tropics (denoted Adjusted N+T).

7  
8  
9  
10  
11  
12  
13  
14  
15

1



2

3 **Figure 11.** Zonal mean profiles of CO<sub>2</sub> at 75°N on 1 April 2010 from the GEOS-Chem 4° x 5°  
4 and 2° x 2.5° simulations. The simulations began with the same initial conditions on 1 July 2009.  
5 The fossil fuel, biofuel, ocean, and biospheric fluxes used in the simulations were scaled based  
6 on the a posteriori scaling factors from the GOSAT XCO<sub>2</sub> inversion. The biomass burning  
7 fluxes, however, were not scaled.

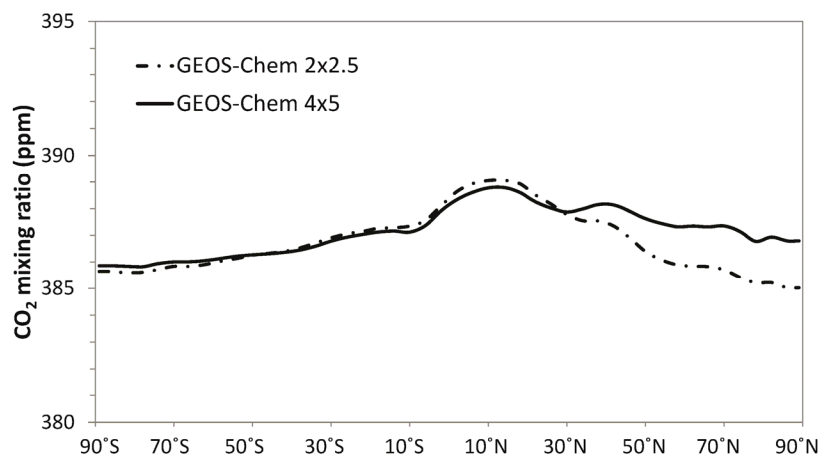
8

9

10

11

12



1

2 **Figure 12.** Latitudinal cross section of zonal mean CO<sub>2</sub> at 12 km on 1 April 2010 from the  
3 GEOS-Chem 4° x 5° and 2° x 2.5° simulations.

4

5

6

7

8

9

10

11

12